

Simulating Transition Cells under the Transition Scale Space Model in Spiking Neural Networks

Simen Storesund

May 1, 2024

Contents

1	Introduction	3
1.1	Animal Navigation	3
1.2	The Transition Scale Space Model	4
1.3	Spatial Cell Types in the Hippocampal Area	5
1.4	Existing Grid Cell Models	7
1.5	Grid Cells as Potential Transition Neurons	9
1.6	Thesis Goal	10
2	Methods	11
2.1	Overall model design	11
2.2	Considering BVC inputs	13
2.3	Rectangularly spaced inputs	14
2.4	Randomly spaced inputs	15
2.5	Multi Compartment Model	16
2.6	Boundary vector cell inputs	17
2.7	Other network models	17
2.7.1	Rate coded inputs	18
2.7.2	Linear Summation BVC model	18
2.7.3	Linear Multi-compartment Models	18
2.8	Simulation software	19
2.9	Analysis	19
3	Results	20
3.1	Defining Typical Parameters: a Standard Model	20
3.2	Gridness scores in the different models	23
3.3	Orientation and phase distribution	26
3.4	Gridness spacing	28
3.5	Temporal stability	29
3.6	Multi-Compartment Models	30
4	Discussion	32
4.1	What this model shows	32
4.2	A word about parameters	34
4.3	Comparison to existing grid cell models	34
4.4	Comparison with existing TSS simulations	35
4.5	The future: benefits of BVCs, biological plausibilities etc	36

1 Introduction

1.1 Animal Navigation

One baffling observation from the study of animal biology and neuroscience is how easily animals are able to grossly outperform human-made robots. This is true over a wide scale: not only are birds able to repeatedly and consistently trek thousands of miles between two locations each year, but a range of animal studies show how for instance mice flexibly and reliable learn to adapt to their novel environments, seemingly using a broad range of environmental cues, as well as self-motion. In 1948, Edward Tolman connected observations of navigating rats to a term he coined a cognitive map (Tolman 1948). This was too early to have any suggestion for the neural basis of a cognitive map, and instead based on how rodents solved certain maze problems.

For instance, in one task described in a 1946 paper, a rat would enter a circular hub from a south arm (Tolman, Ritchie, and Kalish 1946). From the hub, the only other exit was to the north. This exit led to winding corridors and eventually a reward in a location that was ultimately north-east of the starting circular area. After conditioning on this northern pathway and the reward, the rat would enter the circular area to find that the northern path was blocked - instead, a series of radial arms had appeared at different outbounding directions from the hub. Rats, put in this central hub, seemed to prefer radial arms of approximately north-eastern direction, which indicated that what they learnt, during conditioning, wasn't just a stimulus-response reaction, in which they learnt to run straight forward upon entering the hub, do the exact turns needed, and get the reward. Instead, Tolman argued, the rat learned some kind of map of the environment, leading to knowledge of where the reward-location was, relative to the central hub. The more comprehensive this map would be, the more flexibly the rat would be able to navigate the world.

Since then, spatial navigation and cognitive maps has been extensively studied both on a behavioral and a neuronal level, leading to a wealth of observations on how the brain does what human-made robots cannot (Dudchenko 2010). However, since Tolman, some debates have been running as to the extent of this cognitive map, and what drives it. One central topic is whether the cognitive map is formed by path integration or external landmarks, or which one is preferred. Path integration is thought to use proprioceptive and vestibular information to estimate the animal's velocity during movement, which can be integrated in time to form a cognitive map. The benefit of path integration is that it doesn't rely on external senses, and is as such extremely flexible in a series of conditions, but it struggles due to accumulation of noise over time. Remarkably, removing a hamster from their nest in pitch darkness and placing them in the middle of a surrounding open field reveals that they will return directly to their nest. Meanwhile, if the underlying environment is carefully rotated, the hamsters showed a slight tendency to go in the direction their nest would have been before rotation (Etienne 1980). Numerous studies have shown rodents', and other animals', ability to home, or find a straight path from some location to a home location, following spatial exploration. However, pure integration, without any external cues, is only seen to work over short distances in both rodents and humans (source?).

Navigating with external landmarks is also extensively tested. A typical example is the radial

arm maze, in which a rodent is placed in the center of a room with a number of radial arms, typically eight, in which each might be baited with food. Rodents are typically able to extract food by visiting each arm only once, showing some kind of memory of where they have been. However, if given a series of external landmarks, that are placed on walls outside the maze, and these landmarks are either rotated or shuffled after the rodent has visited three out of eight arms, the following performance drops significantly (Suzuki, Augerinos, and Black 1980). The benefit of using external landmarks or sensory cues is that chosen well, they tend to be invariant in time, providing allocentric navigational information. This makes them robust to noise and drift. However, landmarks are only useful as long as these landmarks can be observed.

1.2 The Transition Scale Space Model

The transition scale space model (TSS) seeks to explore how a mental map of the environment could look, from a computational perspective (Waniek 2020). The model goes beyond spatial navigation, but the principles it operates under can easily be extended to a spatial environment, and posits, initially, that any model-based path finding system would require two separate memories: a mental map, or some internal representation of the environment, and some way to connect locations on this map together to get sequential routes between some start and some goal.

While the physical space as experienced by mice is a continuous two-dimensional plane, any cognitive map of the environment must be represented by discrete neurons. This discretization of space could occur in many ways, but matching experimental observations, the TSS model suggests that this map could be a network of neurons in which each represents single locations in an environment. Part of the purpose of this network is storing information about each location, which is central for navigation: during path-planning, a mouse must be able to selectively avoid locations that are considered dangerous, which can be based on experience of those locations. The cell in this map-network representing 'home' would elicit very different responses from the cell representing a dangerous territory, for instance if the mouse has encountered predators there previously.

Such a network does not necessarily contain information about how locations are connected, spatially. Each node, or cell, in the network, does not know its own neighbors. This information is necessary for spatial navigation, and the TSS-model posits that this information can be stored in a separate network. In this network, each cell represents spatial transitions, to give information about which locations are available at a certain distance from a current location. However, due to the considerable number of possible spatial transitions, making each cell represent a single transition would require a high number of cells, so the TSS model instead suggests letting each transition cell represent multiple transitions.

The TSS model asserts that a transition cell can't represent transitions both to and from the same location - the domain of the transition cell, which are the places the transition cell transitions from, and the image, where it transitions to, must be disjunct. Apart from that, each transition cell should represent as many transitions as possible, to minimize the number of cells necessary in a working transition cell network.

This argument sits at the center of the TSS model, because it posits that if a mouse brain

indeed has these transition cells, they would be as efficient as they could be, appealing to the second level in Marr’s three levels of analysis - in a biological network, any cell with a particular purpose should behave as to fulfill that purpose optimally, whatever the purpose is. Through mathematical derivations, the TSS shows that such a transition cell operating under the constraints listed above would have a striking spatial activity pattern. Although the mathematics won’t be reproduced here, the logic behind an optimal transition cell is as following: a transition cell will be activated in all locations within some confined spatial area, referred to as a ‘center’ region, and will represent all transitions from that center to all places in the region surrounding this center, the ‘surround’ region. The transition cell will try to fit as many of these ‘center-surround’ regions into the environment as possible, as long as there is no overlap between center-areas and surround-areas.

Indeed, in the limit of getting as many center-surround-regions into the environment as possible, this transition cell will be active in a periodic, hexagonal pattern in an open environment, which is a solution derived from the sphere-packing problem in two dimensions (Waniek 2018; Kunsch, Agrell, and Hamprecht 2005). With optimal transition cells, all possible spatial transitions from center-areas to surrounding areas can be encoded in a network of only three such cells, highlighting how effectively these cells represent spatial transitions.

A variable in these transition cells is the size of the center- and surround-areas, which in turn would influence the scale of the hexagonal activity pattern. A transition network as described in the TSS-model would work best with multiple separate scales, so larger scales can accelerate the retrieval of paths. In biological systems, where a transition cell has a rate coded activity in a gaussian for each center region, the ideal increment between scales is the $\sqrt{2}$.

On this basis, the TSS model predicts two memory structures in animals: internal map, which consists of neurons representing single locations, and a network of transition cells trying to bundle as many transitions together without spurious transitions. Cells in the internal map-network should activate preferentially when the mouse is in some signature location, and cells in the transition-network should show a hexagonal firing pattern, representing available spatial transitions. This transition-network should also contain transition neurons on different scales, in which the increment from one scale to the next is the $\sqrt{2}$.

1.3 Spatial Cell Types in the Hippocampal Area

The following section will describe experimental results supporting and opposing these predictions made by the TSS model. Already fifty years ago, the place cell was observed in the mouse hippocampus, and this has led to a series of interesting experiments and observations (O’Keefe and Dostrovsky 1976; O’Keefe 1976). Interestingly, the hippocampus was of interest because of its importance in episodic memory formation. The canonical hippocampal pathways divide the hippocampus in three regions that communicate in a feedforward manner: the dentate gyrus receives inputs from outside the hippocampus, and project these to CA3, which is interconnected with recurrent excitatory connections, while also projecting to CA1 (Cherubini and Miles 2015). The main output region from CA1 is the subiculum, which is outside the hippocampus and projects to the prefrontal cortex. Place cells have both been observed in CA3 and CA1, but have not been seen outside the hippocampus.

The place cell typically fires with a rate that is distributed in a gaussian around one or a few locations in the environment, so a network of place cells can encode all positions in an environment (Wilson and McNaughton 1993). One line of evidence that suggests that place cells participate in navigation is sequential activity, observed both during and after navigation. Sequential place cell activity during rest or sleep after navigation, called replay, reflects both sequences of place cells in the order they were active during navigation, or reverse sequences (Wilson and McNaughton 1994). Interestingly, replay occurs during sharp wave ripples, in which the place cell activity is temporally compressed relative to their activity during navigation.

Preplay refers to sequential place cell activity during navigation. During preplay, place cells corresponding to the current location is followed by place cells that will be active a short time into the future, indicating that the hippocampus has some information about upcoming place cells (Dragoi and Tonegawa 2011; Dragoi and Tonegawa 2013).

The hippocampus is also subject to oscillations in the local field potential, prominently in the 4-11 Hz region, called theta oscillations, or just theta. When preplay is viewed relative to theta, the place cells corresponding to the current locations are active at the trough of the wave, while past place cells activate in the descending part of the wave, and future place cells activate in the ascending part of the wave. This phenomenon is called theta phase precession (O'Keefe and Reese 1993; Skaggs et al. 1996; Hafting et al. 2008).

Replay typically occurs during rest or sleep following explorations, in which sequences of place cells experienced prior to rest are activated again, but compressed temporally (Olafsdottir, Carpenter, and Barry 2016). Moreover, combinations of sequences are seen, which seems to produce novel trajectories in an already explored space.

Interestingly, place cells can be active in multiple environments, but they remap independently of each other (Muller and Kubie 1987). This implies that the place cell networks are modulated by the context, but the mechanisms for this are currently unknown.

Grid cells were originally found in the search of afferents to the hippocampus place cell system, first found in layer II of the medial entorhinal cortex (mECII)(Hafting et al. 2005). Grid cells are characterized by periodic spatial activity, arranged so that the firing fields make up hexagonal patterns spanning the environment, and this activity is found both in stellate- and pyramidal cells of mECII(Rowland et al. 2018). These cells are also firing independently of head direction or velocity, and have since been found in multiple other parts of the brain, such as in deeper layers of the medial entorhinal cortex (III - IV), as well as the pre- and para-subculum (Boccara et al. 2010).

Grid cells, too, have received a lot of attention, and a series of details about their firing properties has since been revealed. Grid cells seem to align with the boundaries of their environment with a small wall-angle offset, and grid cells located near each other in the entorhinal cortex also share the spacing, or size of each hexagon. However, along the dorsoventral axis, the spacing of the grid increases by a factor of $\sqrt{2}$ (Stensola et al. 2012). Grid cell activity is strikingly robust across trials and time, and it also seems to persist when visual cues are removed. However, their hexagonal gridness depends on the environment shape, and their firing pattern gets distorted in trapezoid or not-regular environments (Stensola et al. 2015; Krupic et al. 2015).

Grid cells also exhibit theta phase precession during navigation (Hafting et al. 2008), and interestingly, when abolishing the theta rhythm by lesioning the medial septum, grid cell activity loses their spatial correlation in mice, so theta rhythm seems critical for the grid cell pattern (Brandon et al. 2011; Koenig et al. 2011). However, this was not seen in similar experiments in bats (Yartsev, Witter, and Ulanovsky 2011).

The medial entorhinal cortex receives projections from a wide range of cortical and subcortical regions, as well as other hippocampal areas . Notably, the pre- and parasubiculum and the post- and perirhinal cortex are important input structures (Kerr et al. 2007). These regions are important in integrating multi-model sensory input (Furtak et al. 2007; Groenand and Wyss 1990), but to the writer's knowledge, the precise properties of grid cell afferents is not known.

Within mECII, grid cells seem to be interconnected by parvalbumin-positive interneurons, applying strong, lateral somatic inhibition, while excitatory connections have not been observed (Couey et al. 2013; Buetfering, Allen, and Monyer 2014). Moreover, maturation of this interneuron structure seems to reinforce and strengthen the spatial correlations of grid cells (Christensen et al. 2021). Connectivity between grid cells and place cells is only partially mapped, but in addition to the canonical tripartite synapse model, establishing the dentate gyrus as the main input region of the hippocampus, the mECII also projects directly to CA1 (Tamamaki and Nojyo 1993; Kerr et al. 2007; Witter et al. 2017). This suggests that place cells might be formed based on summation of grid cell inputs on multiple scales, but this idea was contradicted when place cells were found to mature earlier in development compared to grid cells (postnatal day 16-17 versus postnatal day 19-20) (Langston et al. 2010; Wills et al. 2010; Wills, Barry, and Cacucci 2012). However, it has been established that CA1 also projects strongly back to mECII, and that grid cell activity depends on these connections (Bonnevie et al. 2013).

1.4 Existing Grid Cell Models

A multitude of models and model families already exist to explain the wealth of experimental data on grid cells, with differences in their suggested mechanisms for the grid pattern, as well as the purpose of the grid cell. Due to their persistent spiking in darkness, many models assume that grid cells do path integration, integrating self-movement information to predict current location in the absence of external input. Oscillatory interference (OI) - models seek to explain the theta phase precession in grid cells, and have shown that grid-like activity can be achieved by the interference of multiple oscillators in membrane potential (Burgess, Barry, and O'Keefe 2007; Zilli and Hasselmo 2010). The OI-model can account for many activity patterns besides the hexagonal grid, but if the different oscillators differ in frequency by a sufficiently small margin, and adapt this margin based on speed- or velocity-signals, the cell can have a grid-cell-like activity with spacings as observed in experiments. Since the theta oscillations typically is one of the interfering oscillations in OI-models, these models reproduce observations of both theta phase precession and the impaired grid cell firing when theta oscillations are disrupted.

Another set of models explain the grid cell as a part of a continuous attractor network (CAN), which can explain persistent grid cell activity during rest or sleep (Yoon et al. 2013; Widloski and

Fiete 2014). These models can be implemented with lateral inhibition between grid cells, as observed in mECII, as long as the strength of the inhibition is inversely proportional to the overlap of firing fields, so the most active grid cell silences all other grid cells. When the animal moves, this activity is shifted to a grid cell with a neighboring phase.

It has been demonstrated that any such system of path integration still needs regular external input to avoid drift (Mulas, Waniek, and Conradt 2016), and the exact inhibitory structure predicted by CAN - networks have not been observed. Additionally, the velocity-based inputs have not been observed, although this might just stem from the unexplored input-space of grid cells (Zilli 2012). However, CAN models fit well with the topological analysis of mECII - activity.

A third group of models predict that grid-patterns can be learnt by Hebbian learning, which is by associating to the right spatial inputs and dissociating from other spatial inputs (Soldatkina, Schonsberg, and Treves 2021). As opposed to the OI- and CAN-models, the driving mechanism of grid cell activity in these feed-forward models is not necessarily self-motion inputs, put that doesn't exclude the possibility that grid cells play a role in path-integration.

An early idea was to model this using firing fatigue, in which grid cells received inputs from cells with rate-based place cell-like activity, although they were not claimed to actually be hippocampal place cells (Kropff and Treves 2008). In this model, there were two primary factors for learning - competitive firing rates between grid cells, so the total population rates were normalized, as well as a firing fatigue, so prolonged firing would reduce rates. Grid cells would then associate to place cell inputs based on their mutual rates, and the fatigue prevented the same grid cell from associating to all inputs. While this produced grid-like cells, carefully tuned excitatory collaterals between gridcells were necessary to make them share orientation. Later, this excitatory collateral was replaced by inputs from a layer of collateral cells that received both place cell-input and head direction-cell input, so the model produced grid cells with shared orientation in a purely self-organized manner (Si and Treves 2013).

Some models produce grid cells with a center-surround learning rule from place-cell inputs. In these models, grid cells typically associate to place cell inputs with firing fields with a given distance, and dissociate from place cells with firing fields outside this distance. Mercade and Leibold showed that this learning rule, combined with lateral inhibition, reduced boundary-effects on grid formation and showed a high level of gridness (Monsalve-Mercado and Leibold 2020). While the grid cells preferred an orientation around 7.5 degrees, in line with experimental results, but all grid cells were found in one of three distinct phases. Another feedforward model added a second ring around the center-surround area, and place cells within this narrow ring were tagged so new firing fields can only occur on the narrow ring. Moreover, if a place cell gets tagged from two separate firing fields of one grid cell, the weights would potentiate. While this was robust to noise, it is unclear if orientations and phases would align between grid cell (Castro and Aguiar 2014).

The observation that center-surround plasticity can lead to gridness is reminiscent of ideas from the TSS model. In the TSS model, the suggested mechanism by which transition cells learn is suggested to be similar to how place cells learn their receptive fields. The place cell learns to activate based on spatially modulated sensory inputs, in which each place cell associates to spatial

inputs from one area, and lateral inhibition prevents other place cells from activating. This has been explored previously, for instance using boundary vector cells as inputs (Barry et al. 2006). Boundary vector cells and other vector-based location cells, such as object vector cells, are similar in that they activate preferentially when the animal is at some distance and direction relative to an external structure. Cells are called boundary vector cells if this structure is an environment boundary, such as a wall or a cliff, while they are called object vector cells if the structure is some environment landmark. Using cells like these as spatial input in a feed-forward network is attractive because the cells can plausibly exist and be configured prior to exploration, and computed during exploration through optic flow (Raudies and Hasselmo 2012).

1.5 Grid Cells as Potential Transition Neurons

The TSS model suggests that while the cognitive map of the environment is the place cell network. The place cell learns to activate based on spatially modulated sensory inputs, in which each place cell associates to spatial inputs from one area, and lateral inhibition prevents other place cells from activating. This has been explored previously, for instance using boundary vector cells as inputs (Barry et al. 2006). Boundary vector cells and other vector-based location cells, such as object vector cells, are similar in that they activate preferentially when the animal is at some distance and direction relative to an external structure. Cells are called boundary vector cells if this structure is an environment boundary, such as a wall or a cliff, while they are called object vector cells if the structure is some environment landmark. Using cells like these as spatial input in a feed-forward network is attractive because the cells can plausibly exist and be configured prior to exploration, and computed during exploration through optic flow (Raudies and Hasselmo 2012).

The grid cells are suggested as TSS transition cells, collectively forming a transition network. As predicted for transition cells, grid cells typically have a hexagonal activity, and are divided in modules based on their scale, which increments by a factor close to the $\sqrt{2}$. To learn these firing fields, TSS posits that transition cells correlate and decorrelate to the same spatial inputs as place cells. As opposed to place cells, transition cells associate to spatial inputs responding to center-regions, and dissociate from inputs in the surrounding-regions, while trying to fit as many center-regions into the environment as possible. This resembles some of the feed-forward models presented above. Similarly to CAN-models, however, TSS suggests that transition cells are interconnected by strong lateral inhibition, to discourage overlapping center-regions.

The connectivity between the place cell network and the transition cell network that enables flexible path-planning is then learnt on top of this, based on correlated place- and transition cell activity.

A learning rule for transition cells has been shown to produce grid cell-like transition cells in discrete-time simulations. In these simulations, transition cell networks consisted of three transition cells, the smallest possible number to cover the entire environment, and the transition cells received spatial inputs sampled from a regular, rectangular grid of spatial cells (Waniek 2017). In discrete time-steps, activity in the spatial cell layer would activate transition cells depending on a position in a simulated trajectory. Following this, three separate learning rules would update input-to-transition

cell weights. The first rule would let the most active transition cell associate to the central spatial cells, and dissociate from surrounding spatial cells. The second rule, called the baseline, would increase the weights from the active input cells to all transition cells, for both active and inactive transition cells. Third, an interaction rule would weaken the connection from inputs to all transition cells except the most active one. A rationale for the three learning rules is that the first rule provides the center-surround effect necessary for transitions, the baseline encourages transition cells to be active as frequently as possible to encourage effective transition cells, and the interaction rule discourages excessive overlap between transition areas.

Although this network gave cells with high gridness in networks of three transition cells, it did not in bigger networks. This is necessary in a biological network. Additionally, it is unlikely that a biological network providing the spatial inputs shows regularly distributed, place like activity, at least prior to exploring the environment. Both of these constraints need to be addressed for this network to be considered biologically plausible.

1.6 Thesis Goal

In this work, the main objective is to build upon the simulations already conducted in the TSS-model, and establish this network structure in a more biologically plausible way, and explore under what conditions or constraints transition cells develop a hexagonal structure.

This task is divided in two. First, to see if a biologically plausible network can contain more than three grid cells, by simulating in continuous time with delayed inhibition, so multiple transition cells can associate to the same place. The network should resemble the previous simulation as much as possible, to allow some level of comparison.

Second, the way the structure of spatial input affects gridness is also explored. This was both to see if using rectangularly spaced inputs was necessary to produce gridness, and to evaluate the possibility of vector-based inputs such as BVCs, instead of place-like inputs. To allow a center-surround learning rule, spatial input was always phase-coded, so the grid cells received pulses of inputs in simulated theta-cycles. Within a cycle, inputs only arrived in a limited time window, and the more spatially relevant inputs arrived earlier. In addition to rectangularly spaced inputs, inputs distributed randomly with either a blue noise or a white noise distribution was also tested.

For highest biological plausibility, though, this input would be boundary vector cells or similar, and this was attempted with complex dendritic computations to allow differentiating vector-inputs. With these different distributions of inputs, the main interest was whether transition cells developed high levels of gridness, and compare it to other results.

With a simple STDP- based learning rule, along with a baseline weight modulation, transition cells developed high gridness levels in larger networks than previously observed, and in with multiple network structures. This is an argument that cells can learn spatial transitions effectively under biologically plausible conditions. However, gridness did not occur in models with BVC-inputs, and more work is necessary to link these observed

2 Methods

2.1 Overall model design

The purpose of this thesis is to test gridness in transition neurons as described by the TSS-model with biologically plausible spatial inputs and conditions (continuous time). To achieve this, transition cells were simulated in a spiking neural network, which are artificial neural networks with certain properties:

1. The network is simulated with continuous time, or in time steps that are vastly shorter than the mean firing rate of neurons.
2. Neurons communicate in temporally discrete spikes, triggered when an internal voltage variable exceeds a threshold.

Different network structures have been tested over the course of the thesis, and the results of different structures are treated in the results section. This section will first describe an ideal network, and describe the different assumptions that network would operate under. The subsequent sections will describe other network structures that were used to simplify and test different levels of plausibility.

An ideal network has the following properties: it is simulated in a biologically plausible setting, such as a spiking neural network. Most importantly, this means that communication happens with delays, time is continuous, and learning rules must be online and local. Online and local learning rules mean that all variables necessary for learning must be available at the time of learning (online) and in the physical location where learning occurs, typically the synapse (local).

Spike timing dependent plasticity (STDP) is a learning rule in which a synapse updates weights both when the presynaptic and the postsynaptic neuron spikes (source here?). The weight-update is according to a STDP-kernel, in which weights are decreased upon presynaptic activity and increased on postsynaptic activity. The magnitude of weight decrease is high if there was a postsynaptic spike shortly before the presynaptic inputs, and the magnitude of weight increase is high if there was a presynaptic spike shortly before postsynaptic activity. The processes of decreasing and increasing weights do not need to be symmetric. STDP is a learning rule that satisfies the rules above.

A baseline learning rule increments weights slightly when a presynaptic neuron is active, regardless of postsynaptic activity. This learning rule is also online and local, satisfying all constraints.

Next, ideal simulations get inputs from some plausible spatially tuned neurons, more precisely boundary vector cells (BVCs), whose activity is based on real or simulated trajectory data. From these inputs, another layer of cells of arbitrary size learns center- and surrounding area information to represent transition-cells as described in the TSS-model, encoding transitions on a single scale. Under these constraints, the objective is whether the transition neurons self-organize into single-cells with hexagonal activity patterns in space, and in which the population covers all possible environment transitions on a given scale.

Finally, an ideal network is not dependent on highly specific parameters, and shows some robustness to noise, which is likely necessary for any actual brain network.

Both an ideal network and subsequent simplifications will have some common features to accommodate these objectives: first, spike timing dependent plasticity is a biologically plausible learning rule which both allows single transition cells to associate with spatial inputs associated with center, and dissociate with inputs associated with surround areas. To facilitate this, all inputs arrive in pulses at theta-wave frequency, 10 Hz, in which only spatial input with sufficient relevance is active (Figure 2.1 a & b). The input is also phase coded, so the less relevant, the higher the temporal offset is relative to theta. This means that a transition cell is likely to fire following center-inputs, and following receive a burst of inputs from cells representing surrounding locations. The STDP learning-rule will encourage potentiation of the center-activity, which arrived pre-spike, while the surround-activity arriving post-spike is depressed. Secondarily, all active inputs are slightly potentiated to encourage the transition cell to be active in as many center-areas across the environment as possible, according to a baseline-learning rule.

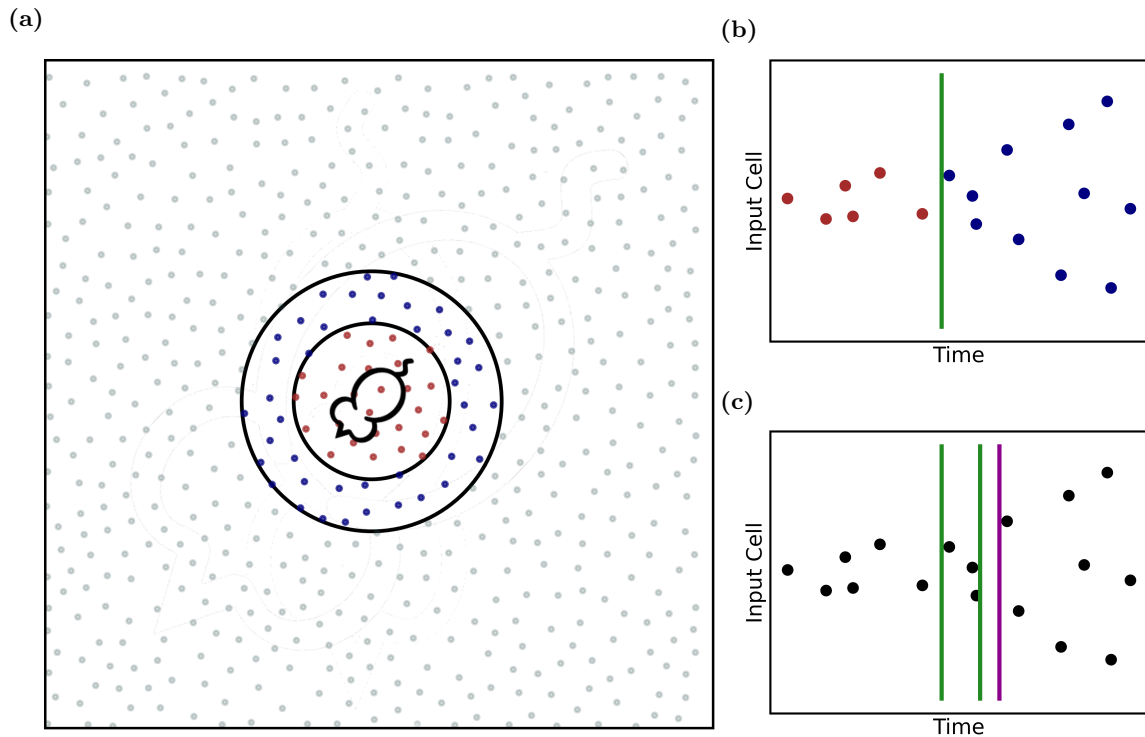


Figure 2.1: The nature of phase coded spatial inputs. (a) Spatial inputs from a region surrounding the mouse will be activated each theta-cycle (10 Hz), here indicated by points within the two surrounding circles. This input is phase-coded, so cells responding to locations closest to the mouse will activate first. (b) Hypothetical raster plot showing input activity in one theta cycle. The spike time of a transition cell spike (green vertical line) determines which inputs the transition cell will associate to and dissociate from. In this case, the transition cell associates to the inputs colored red (left of the vertical line), and dissociate from the inputs colored blue (right of the vertical line). Comparing to the input's locations in (a) (color coding preserved), this becomes a center-surround learning rule. (c) Delayed inhibition (purple vertical line, rightmost) can allow multiple transition cells (green vertical lines, middle and left) to fire during the same theta-cycle.

An inhibitory layer connects transition cells laterally, causing strong inhibition, but on a delay. This leaves a narrow window in which multiple transition cells can fire, followed by complete inhibition, so some transition cells partially associate to the same areas (Figure 2.1 c).

2.2 Considering BVC inputs

One goal of this work was to obtain grid cell-like transition cells with BVC inputs, and the simplest way to do this is with a direct connection between the two, so transition cell activity is based on linear summation of BVC inputs. There are reasons to think that such a network is difficult to achieve. The following idea explains this: in square environments, one could imagine picking two locations that the transition cell has associated to, denoted (x_1, y_1) and (x_2, y_2) , and that should make up two firing fields in the hexagonal pattern. In locations (x_1, y_2) and (x_2, y_1) , the input would be highly similar to half the input from position 1 and half the input from position 2, due to the nature of BVCs. Notably, though, the transition cell should not fire in these locations, because that would lead to rectangular grid firing patterns, not hexagonal. This would be true for all pairs of firing fields that are not parallel to one of the walls. In other words, square environments and linear summation of BVC inputs encourage rectangular fields, not hexagonal.

It should be noted here that the spiking neural network itself implies non-linear features that might have enabled such a network to produce grid-cells. One way to achieve this would be with other transition cells that are sufficiently active in location (x_1, y_2) and (x_2, y_1) , so they inhibit the first transition cell. However, due to the fine-tuning such a network would require, this network structure was not pursued further.

An interesting alternative, which highlights an advantage of biological neurons over simplified artificial ones, appears after considering nonlinear dendritic computation on transition cells in a multi compartment model. With this in mind, although boundary vector cells technically synapse onto transition cells directly, the simulation treats dendrites as separate units within one transition cell. Each dendrite would get inputs from some subset of BVCs, and the transition cell can associate and dissociate to all inputs on an entire dendrite. Similarly to the BVC-model (Barry et al. 2006), each dendrite would preferably be active in only single locations in the environment. This could be achieved by for instance responding non-linearly to BVC-inputs with a soft-max activation function. In the example above, this would let the transition cell associate to dendrites responding highly to (x_1, y_1) or (x_2, y_2) , while remaining dissociated from dendrites activated in (x_1, y_2) or (x_2, y_1) , without sacrificing biological plausibility. This multi compartment model is in line with the ideal model described in section 2.1.

However, to shorten simulation time and reduce complexity, this kind of network can be simplified. This can be done incrementally, in which each step simplifies complexity but also reduces plausibility:

1. The BVC-model showed that place-like activity can be produced from BVC-inputs. As such, BVC-input can be replaced by place-like inputs directly as non-spiking dendrites in the multi-compartment model.
2. To reduce the number of neurons, each dendrite can connect to each grid-cell, and the dendrites can be spiking to reduce computational time for each of them. Here, the dendrites still fire in random places, according to some distribution.
3. The dendrites can respond to places distributed in a regular, rectangular grid.

Note that step 3 is highly similar to the already existing simulations by Waniek (citation?), just here in a spiking neural network. This was useful, because it allowed testing the hypothesis that transition cells can produce grid-like behavior in networks of more than three neurons if the inhibition is delayed, not showed in previous simulations. Then, networks could gradually be made more complex and biologically plausible, leading to a series of networks that could be tested sequentially from simple and less plausible to more complex and more plausible. The concrete implementation of each network and other considerations are treated in their own upcoming subsections.

2.3 Rectangularly spaced inputs

This network structure carries significance in this work for two reasons: it is closely related to previous TSS-simulations, and is an ideal place to investigate if larger networks still give gridness. Moreover, as outlined in section 2.2, it provides a useful stepping stone to subsequent models.

The network has three main layers: input neurons, transition cells and inhibitory neurons. The input neurons have a preferred spatial location, and have the chance of being activated each theta cycle, which is set to happen with a 10 Hz frequency. The activation function for input neuron i with position (x_i, y_i) is given in equation 1.

$$\text{delay} = \frac{\sqrt{(x_i - x)^2 + (y_i - y)^2}}{\sigma} + \mu \quad (1)$$

Here, x and y is the current location, σ is a scale parameter determining the width of input, μ is noise and delay ends up in ms. Typically, there was a cutoff at 20 ms, so only reasonably active inputs would activate, but this cutoff was arbitrary, and could for instance depend on the transition cell scale. In this model, inputs would be distributed in a rectangular, even grid across the environment.

Each of these inputs synapsed on each transition cell, with weights initialized randomly from a uniform distribution, between 0 and some maximum, w_{max} . The transition cell had a voltage parameter which triggered spikes if it surpassed a threshold, or updated according to 2.

$$v(t+1) = \begin{cases} 0, & \text{if } v(t) > \text{threshold or refractory} \\ v(t) - e^{-(v(t))/\tau} + \sum_0^i (w_i \cdot i(t - \text{delay})), & \text{otherwise} \end{cases} \quad (2)$$

Here, $v(t)$ is the voltage of time, τ is a decay parameter, w_i is the weight of the i th input and $i(t - \text{delay})$ is 1 iff input i spiked at time $t - \text{delay}$, in which time is the input delay.

The STDP learning rule was implemented by separating potentiation and depression: upon transition cell firing, potentiation for weight i would increment dependent on presynaptic activity (3).

$$w_i = \text{clip}(w_i + a_i^{pre} \cdot \nu, 0, w_{max}) \quad (3)$$

in which a_i^{pre} is a variable incremented when input i fires, and decays with time. ν is here a learning rate, which can be constant or modulated by animal velocity. Similarly, upon presynaptic input from input i , weights are depressed if the input arrives after transition cell spike. Regardless of transition cell activity, the input weight would also increase according to a baseline parameter. Both of these rules are captured in equation 4

$$w_i = \text{clip}(w_i + (a_i^{post} + \alpha \cdot (w_{max} - w_i)) \cdot \nu, 0, w_{max}) \quad (4)$$

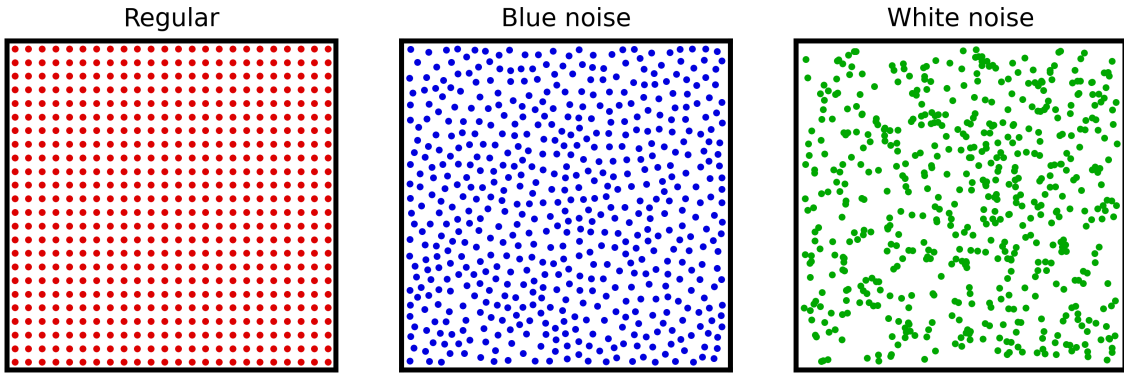


Figure 2.2: Examples of the three kinds of input distributions. Each plot shows 24x24 inputs. Regular distribution places inputs evenly across the entire environment in a rectangular way. A blue noise distribution places inputs sequentially so each is placed as far away from previously placed inputs as possible, resulting in an even, unstructured distribution. White noise distribution places inputs randomly, and independent of all other inputs, so some locations produce more input activity than others.

where a_i^{post} is a symmetric parameter to a_i^{pre} , but which decrements upon post synaptic firing and decays at a separate rate. α determines the magnitude of baseline weight increase.

Transition cells then interacted by activating inhibitory neurons which inhibit all transition cells for a time, working by reducing their voltage by a large, constant amount, but which was small enough so the voltage returns to zero by the next theta by equation 2. This inhibition was global and uniform, so each transition cell inhibited all the others and itself equally. Although this inhibition was thought to work with a delay, some simulations tried running without. In these, the delay was at the simulation software's minimum, 0.2 ms. The number of transition cells in a simulation was arbitrary, but typical values chosen were 13, 23 or 37.

2.4 Randomly spaced inputs

This network structure had similar structure and learning rule to the network in section 2.3. In these networks, however, there was some randomness in determining which area an input neuron responded to. This was specifically done to investigate if rectangular inputs were a necessary component in developing gridness.

This was tested with two separate input distributions, in addition to the rectangular grid given in section 2.3 (figure 2.2): One, the inputs were distributed in a blue noise like pattern, to ensure a relatively even, although not regular, distribution of spatial firing. Two, the inputs were distributed in a white noise like pattern, in which one input neuron would respond to areas independently of other areas. Considering the multi-compartment dendrite model mentioned previously, a white noise pattern might be most natural, because it meant that each input receptive field can be placed independently of other fields. However, it has the disadvantage that some regions in the environment will be more or less densely covered by inputs, so a transition cell that's supposed to fire in some region according to its grid might not receive any dendritic input there at all. Blue noise, which broadly speaking places the location of each spatial input as far away from every other inputs as possible, with a random element, will provide approximately even coverage of the environment.

The blue noise inputs was generated by iteratively suggesting a number of uniformly distributed

points, adding the point that was the furthest from all previously added points to the added points, and repeating until the desired number of added points was reached. To allow for good spreads, the number of suggested points was directly proportional the number of existing points. White noise inputs were generated by getting the desired number of uniformly distributed points independently of each other.

2.5 Multi Compartment Model

A multi compartment model was briefly justified earlier, as a way to include non-linear dendritic computations which were interesting for BVC-inputs. The most natural way to implement this in the simulation software used was as a separate, non-spiking layer between the input-layer and the transition cell layer, and simulate the synapses from dendrites to transition cells as gap junctions. Although this was thought to take BVCs as inputs, an intermediary step would be to keep place-like inputs, but see how transition cells developed with this non-spiking intermediary dendrite layer.

To justify the two-layer neuron model with dendrites and soma as a multicompartment model, the dendrites had the following properties: they only synapsed onto a single transition cell bodies, were non-spiking, and the dendrite-to-soma connectivity was modelled as a gap junction, as in (reference). In this model, each dendrite only received input from a single input neuron, to simulate the place-oriented dendrite. Each dendrite had a voltage-parameter that would increment by a factor w when receiving inputs, and decaying to 0 over time (equation 5):

$$v_{den}(t+1) = v_{den}(t) + e^{-(v_{den}(t))/\tau} + \sum_0^i (w \cdot i(t - delay)) \quad (5)$$

This resembles 2, but does not have the option of setting voltage to 0 above some threshold, as the dendrite is non-spiking. In terms of inputs, with place-based inputs, each dendrite would only receive input from one input neuron. The weight w would be a hyperparameter, not changing during a simulation, and was equal for all dendrites.

Based on this, the grid cell's voltage was determined by the following equation 6.

$$v_{soma}(t+1) = \begin{cases} 0, & \text{if } v_{soma}(t) > \text{threshold or refractory} \\ \sum_i c_i \cdot \tanh(v_i), & \text{otherwise} \end{cases} \quad (6)$$

Here, the nonlinear function $\tanh(v_i)$ gives the dendrite a softmax-like behavior, so the dendrite at anytime is either activated or not, dependent only on its internal voltage-parameter. v_i is the voltage of dendrite i , c_i is the corresponding dendrite conductance, reflecting how effectively the dendrite's voltage affects the grid cell voltage. The learning rules 3 and 4 is here learning over conductances instead of synapse weights, but is otherwise identical.

With this network structure, simulation times were significantly higher than with direct connection between input cells and transition cells, because the number of dendrites was the product of the number of input cells and the number of transition cells. This limited the amount of time spent on this and subsequent models.

2.6 Boundary vector cell inputs

This network structure was designed to be as biologically plausible as possible, but it builds directly on section 2.5. Similarly to the model described above, inputs would synapse on an intermediary layer of dendrites, which would activate according to a softmax - function, which in turn would influence the spiking of the transition cell. Each dendrite would receive some subset of BVC-inputs, and the softmax function would be tuned so receiving only one or a few inputs would not elicit any dendrite activity.

From observations with different input distributions, there were reasons to think dendrites would respond to single locations, and in which the collective dendritic tree would respond evenly across the environment, such as with regular or blue noise-based input distribution. One way to do this would be by having dendrites receive a superfluous number of BVCs, and during exploration associate to some number of these so the dendrite would only respond to some location, while having dendrites avoiding to associate to the same area. However, this was not pursued further due to significant complications.

Instead, a simplified version was used, in which BVCs responded preferentially to one of only two directions: north and east, with a series of different distances. Then, each dendrite received a pair of inputs, one from north and one from east, and the BVCs were carefully paired to give the dendritic tree an evenly spaced, rectangular input field. The activation function for a BVC was simply the distance to the wall in the preferred direction, converted linearly to temporal delay.

The multicompartment model was a modified version of the one in section 2.5. While dendritic voltage was the same (equation 5), the softmax-function was here replaced with a hard step-function to simplify simulation times (equation 7):

$$v_{soma}(t+1) = \begin{cases} 0, & \text{if } v_{soma}(t) > \text{threshold or refractory} \\ \sum_i c_i \cdot (v_i > v_{threshold}), & \text{otherwise} \end{cases} \quad (7)$$

This is similar to equation 6, but the dendritic conductance c_i is multiplied by a boolean which is 1 only for voltages above a threshold, $v_{threshold}$. Considering that each dendrite only received two BVC inputs, $v_{threshold}$ was typically between 1.2 and 1.5 times the BVC-to-dendrite weight.

This also necessitated a change in the STDP-learning rule, since a_{pre} would increment not when the dendrite received an input, but when it passed the threshold $v_{threshold}$.

This model is designed to almost forcibly turn BVC-inputs into a model that resembles the first model described in section 2.3: rectangular inputs by carefully pairing orthogonal BVCs on dendrites, and a dendritic model that has replaced a soft-max learning rule with a step-function. Despite these simplifications, which might be justified as a proof of concept for BVC-inputs, this model did not yield gridlike transition cells like the previous models, so further exploration was halted.

2.7 Other network models

A few other network structures were tried apart from the methods above, but were not explored further because they didn't produce the wanted model dynamics. This section will describe the

incentives behind these structures, and how they work.

2.7.1 Rate coded inputs

One structure was designed as an alternative to using phase-coded inputs. The model still relied on dense inputs, so in each position numerous inputs would be active, but their activity was rate-coded. In the spiking neural networks simulated, neurons would always normalize to some base-voltage without external influence, and this model made rate-coded inputs by setting base-voltage depending on animal position. For relevant spatial inputs, the base-voltage would end up above threshold, leading to spiking dynamics. Very active neurons would reach this threshold faster, because the base-voltage would be significantly above threshold.

For a rate-code like this, a transition cell would provide a feedback-signal to the input layer after spiking, which would be weak, only activating almost-active input cells at that time. Coupled with a STDP learning rule, this network structure allowed transition cells to activate the surround-inputs themselves, which would force a post-pre spike timing, leading to dissociation. A challenge with this model was keeping the input structure stable, so there would be some gap between the surround-input activation and the next round of center-inputs. However, with single-cell networks, some measure of center-surround fields was achieved, so the model might technically be viable.

This network structure was abandoned because having feedback-connectivity from transition cells to input cells would have unwanted implications for the TSS-model as a whole, giving the transition cells sway over input activity.

2.7.2 Linear Summation BVC model

The simplest model with BVC-inputs to transition cells would use transition cells as simple LIF-neurons, integrating BVC-inputs and learning directly on the weights from these. Motivation for why this model was abandoned was given earlier, but this model was tested briefly nonetheless. One way to test the stability of the model was to artificially initiate the network with optimal weights, and see if it maintained the necessary firing dynamics. This was done by reverse-engineering weights, creating ideal firing patterns for each transition cell. Then, weights were set by iterating over a 48 x 48 grid of the environment and increasing weights from inputs relevant to a firing position, decreasing weights from inputs that were irrelevant. This approach was not tried for any other methods, but when it failed to give the wanted spiking dynamics in the network, along with the arguments presented in section 2.2, this approach was abandoned.

2.7.3 Linear Multi-compartment Models

Models described in section 2.5 used a multi-compartment model of the neuron to allow dendritic computation to convert vector-based inputs to place-like inputs the transition cell could learn transitions on. In those models, the voltage in a dendrite is transformed to a voltage in the transition cell body through a nonlinear softmax-function, but using a linear conversion was also tried. In this model, the transition cell body voltage was the sum of all dendrite voltages multiplied by

conductances:

$$v_{soma}(t+1) = \begin{cases} 0, & \text{if } v_{soma}(t) > \text{threshold or refractory} \\ \sum_i c_i \cdot v_i, & \text{otherwise} \end{cases} \quad (8)$$

This model was discarded for not showing the necessary dynamics: with BVC-inputs, a number of dendrites were slightly active in a lot of locations, participating in transition cell activity. Even if the learning rules were thresholded, so the STDP- and baseline-learning rules would only apply to moderately active dendrites, this errant activity would mean transition cells would activate in too many consecutive locations, losing circular firing fields.

2.8 Simulation software

All models and implementations can be found on github(Insert link here?), and while the simulation data is not available on github due to storage capacity, it is available (somewhere else?). All simulations were implemented in python, using the Brian2-library for its flexibility and easy implementation (Stimberg, Brette, and Goodman 2019). With this framework, setting up simulations was straight forward, and allowed time-improvements such as only updating STDP-variables when relevant events occurred, not at every time step. Time steps were typically at 0.1 ms, which was also the minimal synaptic delay.

Simulations with place-inputs used self-written simulated trajectories, simulated with 10 ms time steps and a square environment. Position was treated like a continuous variable, with velocity and rotational velocity determined by normal distributions from one time step to the next. In simulations using boundary vectors, the external RatInABox library was used (George et al. 2024).

From the trajectories, spatial inputs were calculated prior to simulations, using either position- or boundary information, and added to a brian2 spikeGeneratorGroup. The network state and weights was stored frequently during simulations.

2.9 Analysis

To investigate the firing properties of the network of transition cells, weights were frozen, and the activity of the network was sampled from each position in an even 48 x 48 grid across the environment. In simulations with noise, each position was sampled 5 times, while they were sampled only once without noise. This gave momentary pictures of the network state, which were subsequently stored as spike trains and then converted to histograms of spatial firing fields. Due to the time it took to get one sample, each simulation was typically sampled each 5 minutes of simulation time.

Five primary variables were derived from each simulation: gridness score, spacing, orientation, phase distribution and temporal stability.

The measure used to evaluate the hexagonality of the transition cells was primarily the gridness score. To find this score, an annulus was extracted around the center of the autocorrelation of the spatial firing fields of a sample. The size of this annulus was estimated to find the first ring of maxima around the center. Using this annulus, gridness score was determined as

$$gscore = \min(a_{60^\circ}, a_{120^\circ}) - \max(a_{30^\circ}, a_{90^\circ}, a_{150^\circ})$$

in which a_{n° is the correlation between the annulus and itself rotated n degrees.

Gridness spacing was found by evaluating the gridness score with multiple estimations of annulus size, and determining values that gave the highest score. Because of the discretization of space, multiple spacings would give similar scores, in which the mean was taken.

Orientation was determined only in cells with a positive gridness score. Orientation was determined as the angle between the horizontal line and the first maxima within the annulus, extracted similarly to in the gridness score.

Phase distribution was only evaluated for cells with positive gridness and an orientation between -5° and 5° , as this seemed to be dominant for most simulations. In simulations with multiple cells passing these criteria, one cell was chosen at random as a basis for comparison. All other cells would be evaluated relative to this basis by doing a cross correlation, and finding the maximal value. To find all positions relative to the rhombus, the phase-difference was unsheared, so the rhombus would be a rectangle. Then, phase differences could be reduced to the within the rectangle by a modulo-operation, and sheared again to be placed within the rhombus.

Temporal stability was estimated by getting the variance in pixel-values in spike plots across time for each cell in the latter half of a simulation, and comparing the mean variances to the mean variance of shuffled pixel values. This approach was enabled by the sampling scheme, in which each location in the environment was sampled equally at even time points. Shuffling the spike plots represented the expected temporal stability if there would be no correlation from one timepoint to the next, while a lower variance would imply a positive correlation of firing fields from one time to the next. [add a figure to show this, as well as other features?]

3 Results

3.1 Defining Typical Parameters: a Standard Model

A few models were tested in this work. In most of these, overall network structure was kept the same, varying instead on certain parameters that were perceived as critical: the distribution of inputs, inhibition delay, the number of transition cells in a network and the role of noise in the spatial inputs. In addition to these variants, this section will show results from a multi-compartment model with non-spiking dendrites, both with place-like inputs and boundary vector cell inputs. Most hyperparameters were not tested, or not tested thoroughly, for reasons related to time constraints. In that light, this section will describe typical parameters of one model, and some of the considerations made in setting some of the parameters. This set of typical parameters ends up making out a standard model, which will be used as a baseline for comparison in the rest of the article. This model was chosen as the base model for comparison because it is closest to previous simulations of the models run in this work.

Table 3.1 shows a typical set of hyperparameters, partially chosen to be biologically plausible, but some sets of parameters were calibrated in order to achieve a wanted dynamic. Since the input was phase-coded relative to theta, weights and spiking threshold were set so the first transition cell would spike typically about halfway between the first input and the phase-delay cutoff. This was

thought to encourage even center- surround fields under a STDP learning rule. Inhibitory delay was set to give a brief window for other cells to fire, and is probably shorter than expected biologically [source?]. The apost, apre and baseline was set up to work in conjunction so potentiation and depression would approximately balance each other out, according to equations 3 and 4. This model also assumed zero noise in the phase delay for simplicity, but different levels of noise was tested in different models.

Table 3.1: Example parameters for simulations. The parameters are partially chosen for biological plausibility, and partly adapted to achieve desired firing dynamics.

Parameter	Value
# Transition cells	13
# Inputs	576 (24x24)
Theta rate	10 Hz
Phase-delay cutoff	20 ms
σ	0.012
μ	0
Transition cell threshold	1.0
Transition cell τ	10 ms
w_{max}	0.14
w_{init}	uniform[0-0.75 · w_{max}]
A_{pre}	0.01
A_{post}	-0.007
τ_{pre}	8 ms
τ_{post}	80 ms
Baseline	0.005
Inhibitory delay	0.6 ms

The simulations were run on a simulated trajectory, as described in the methods, using a one meter by one meter square environment. While weights and parameters were stored mid-simulations, data was also extracted from each model by sampling each position in a grid after freezing learning. For a network with parameters from table 3.1, typical spike plots are shown in figure 3.1.

Clearly, transition cells typically develop center-surround fields quickly, evidenced already after 5 minutes of exploration from random initial activity patterns. Looking at the temporal development of spike plots, while it seems like firing fields are somewhat stable in time, the development of hexagonal gridness is gradual.

Five primary variables were quantified about transition cell activity, all using these spike plots. The primary one is gridness score, which quantifies the degree to which the firing fields are hexagonal. One caveat of the grid score is that it is highly sensitive to shearing and rectangular patterns, so

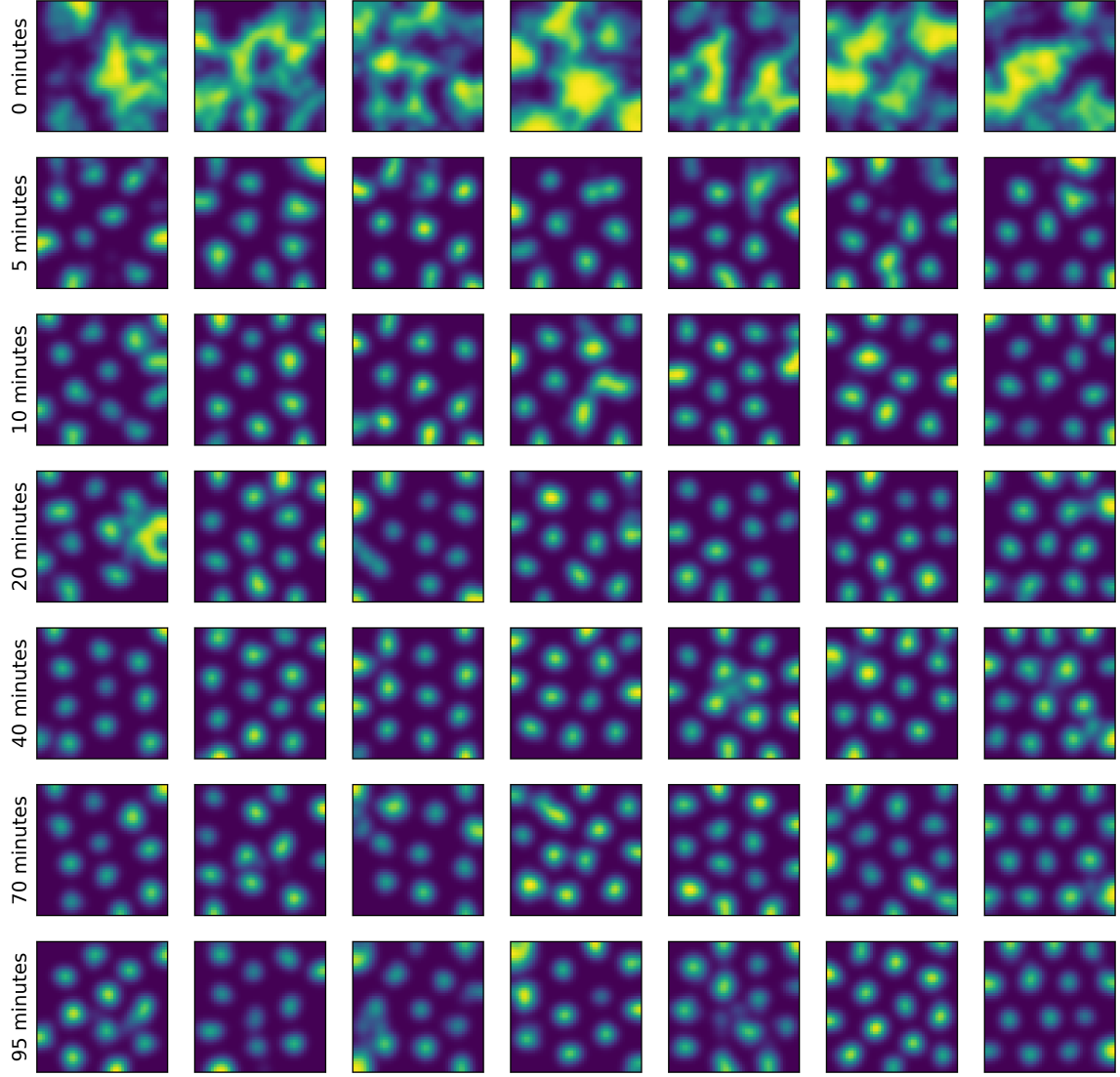


Figure 3.1: Sampled activity from seven transition cells in the same network throughout a simulation. Each plot represents activity in the same 1×1 m environment, subdivided into a 48×48 grid in which each position was sampled for a single theta cycle. Learning was disabled during sampling. Bright spots in the plots represent locations in which a transition cell was active, and each plot is smoothed with a gaussian filter. This sampling method is used for all models, although the number of samplings per position depended on noise levels.

transition cells with distinct periodic firing fields, but without strict hexagonality, can have highly negative grid scores.

The three primary variables for looking at grid cell populations was also used for these transition cells: grid spacing, orientation and phases.

Finally, a measure of temporal stability says something about whether the network converges to some state or is shifting.

The following sections will outline results according to these five parameters for ten models: A standard model with parameters outlined in table 3.1, two models with similar parameters but different spatial input distributions (blue noise and white noise distributions, see figure 2.2), networks with more transition neurons (23 and 37 cells), networks with minimal inhibitory delay (0.2 ms, but referred to as 'no delay') and networks with different levels of input noise.

Input noise occurred in the phase-delay of the input. Each theta cycle, each input had an expected delay depending on its spatial relevance relative to the animal's current position. In each model, the actual delay on an input was modelled as normally distributed around this delay, with standard deviations of 1, 2 or 4 ms. All maintained a 20 ms temporal window each theta cycle.

In addition to these models, a multi-compartment model with parameters similar to the standard model was tested as a proof of concept, referred to as the MC Model. This model also used place-like inputs, but these inputs synapsed on non-spiking dendrites, each dendrite only receiving inputs from one input cell, and each dendrite subsequently affecting the transition cell spiking in a gap-junction-inspired way.

3.2 Gridness scores in the different models

The central question to this work was whether the network structure and learning rule described in the methods section could produce transition cells with a hexagonal firing patterns, which can be quantified by the gridness score. This gridness score was always computed on spike plots such as those shown in figure 3.1, sampled evenly across the environment with frozen weights. This was tracked in ten different network models, each simulated thirty times and sampled every five minutes across a 95-minute simulation. Figure 3.2 a shows final mean gridness score for each simulation, grouped by model, while figures 3.2 (b-e) show the temporal development of gridness scores in the ten models according to groups.

While the standard model as described here produced highest scores, multiple other models had comparable scores. Networks with blue noise-distributed inputs, or with 23 transition cells, or with 1 ms noise, had comparable final griness, and developed approximately equally quickly. The multi compartment model also had high gridness, but not comparable to the above-mentioned groups, which was also true for simulations with 37 transition cells, minimal inhibition delay or 2 ms noise. Finally, white noise inputs performed worse, while having some positive gridness, and 4 ms input noise did not produce stable hexagonality at all.

Despite the differences in gridness, virtually all cells across all simulations seemed to develop clear, isolated firing fields, and fired in multiple locations across the environment. This is true when for instance looking at the firing plots of white noise inputs or minimal inhibitory delay. This reflects

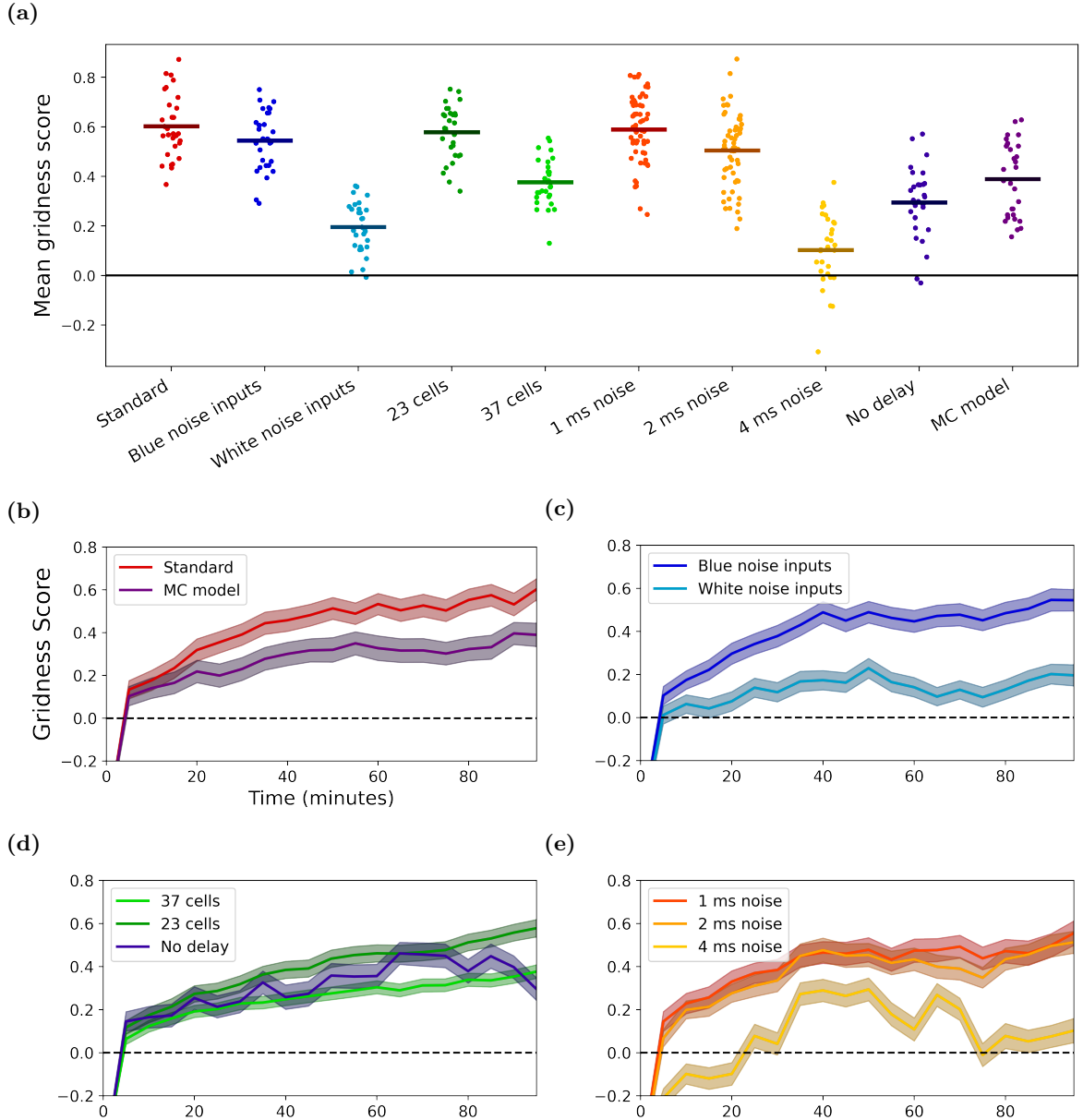


Figure 3.2: Gridness scores for ten model types. (a) Each scatter point represents mean gridness in one simulation after 95 minutes simulation time. Bars are means across all simulations for one type. (b-e) Loosely grouping the model types into four or five main categories. Colors are maintained from (a). (b) The multi-compartment (MC) model shares important parameters with the standard model; they both have networks of 13 transition cells, no input noise and rectangularly spaced inputs. The standard model seems to outperform the MC Model, but both show clear gridness. (c) Models receiving inputs from a blue noise distribution have approximately equal gridness to the standard model, while transition cell networks receiving white-noise inputs do not seem to have the same development. (d) Transition cells exhibit clear gridness both with minimal inhibitory delay and with different network sizes. While a network of 23 transition cells see the same gridness as the standard model, 37 transition cells have a somewhat reduced gridness. Without inhibitory delay, gridness is also reduced, and less stable. (e) While simulations with normally distributed input noise and std 1 or 2 ms have gridness comparable to the noiseless standard model, a std of 4 ms in input noise is not as robust.

some inability in the learning rule to encourage tight bundling of firing fields, which is also reflected in the standard model when the baseline learning parameter is set to 0 [preliminary results, check these later](also, ref some figure here?).

In all models, within-simulation variance in gridness was high, and virtually all simulations had some cells with a negative gridness score at all times (figure 3.3). Low gridness scores can be explained by grid shearing or firing fields that aren't evenly distributed across the environment, while negative scores tend to reflect rectangularity. [I should probably investigate if cells with negative scores tend to have negative scores across a simulation].

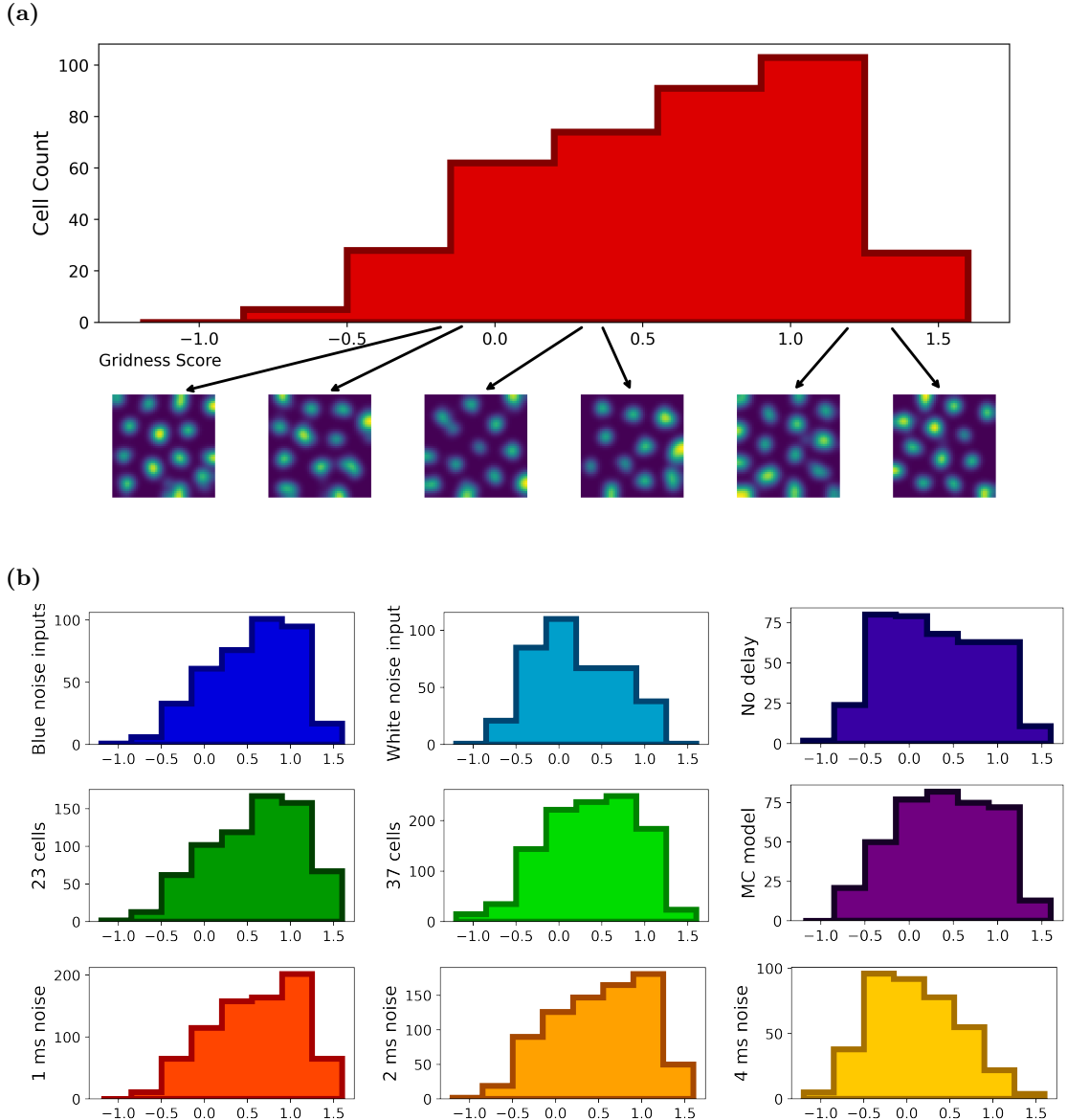


Figure 3.3: Distribution of gridness scores in the different models. (a) Standard model gridness distribution with spike plot examples. Although the mean gridness of this model is considered high (above 0.6), most simulated networks contain cells with negative or low gridness score. Negative gridness is typically produced by rectangular patterns, as shown in the two leftmost spikeplot examples. The two middle examples show activity in cells with positive, but low gridness scores. To have a gridness score above 1, the hexagonal pattern must typically span the whole environment without shearing or rectangularity. (b) Gridness score distributions for the remaining nine models.

Interestingly, the distributions of grid scores can also reflect features of models with lower gridness

scores. The models with minimal inhibitory delay seem to have a wide variety in gridness, so some cells are highly gridlike and others highly un-gridlike, while models with white noise inputs have a higher mode, but rarely sees highly hexagonal cells. In the latter case, it might seem like the cells don't pack firing fields closely enough to develop high gridness, while in the former the between-transition cell competition might be too high to support large networks with high hexagonality.

3.3 Orientation and phase distribution

According to experimental data, grid cells in a module align in orientation with a wall-angle offset of 7.5° , which was also observed in previous simulations of the TSS-model with related learning rules. Grid cells with similar spacing and orientation have phases that are evenly distributed on the toroidal manifold the network is active on. Here, orientation was only computed for transition cells with positive gridness, and normalized to a value between 0 and 60° . Phase distribution was only computed on cells that aligned with the dominant orientation of that model so phase distribution could be accumulated across multiple simulations, and normalized to position within a rhombus of the environment.

In all simulations, the preferred orientation was around 0° , which indicates that transition cells align firing fields preferentially parallel to one of the environment walls (ref figure). However, this wasn't a strong preference, at most one in four cells with positive gridness showed this directionality. Models with noise had less of an orientation preference, as was the case for models with no inhibitory delay.

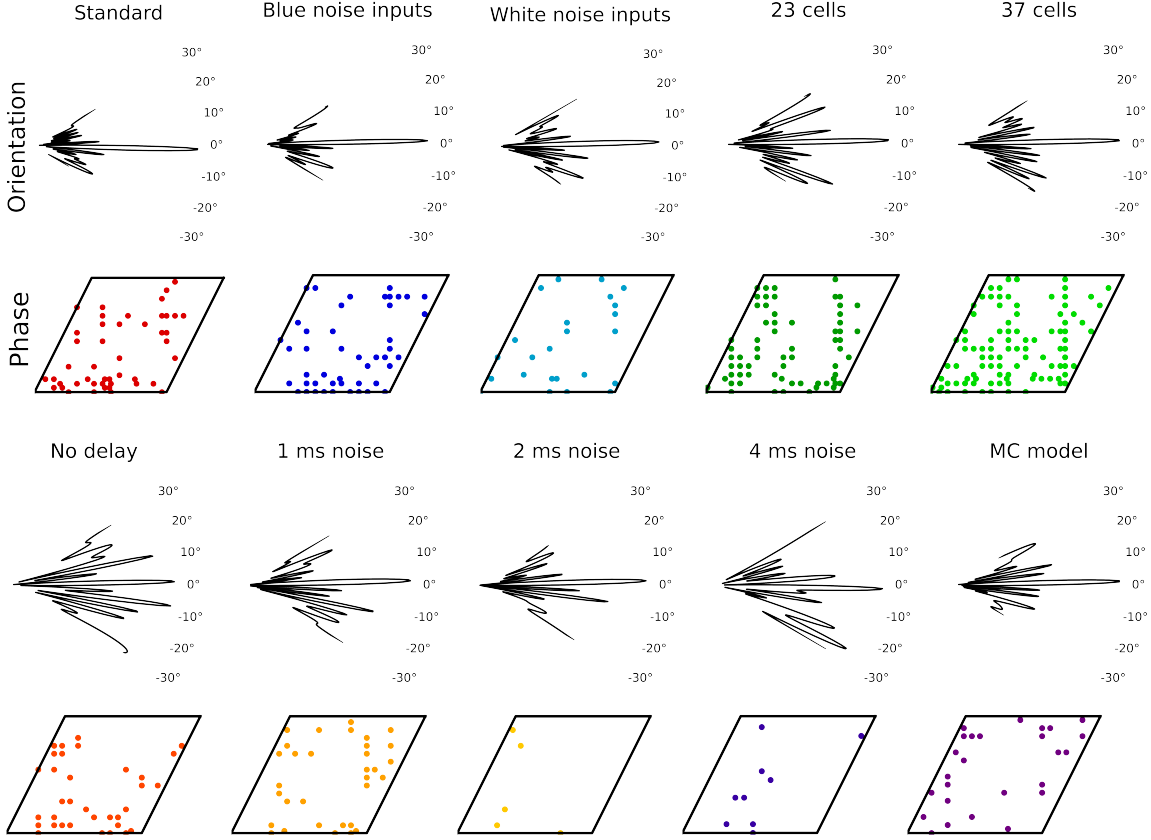


Figure 3.4: Orientations and phases of all models. Transition cells prefer a 0° orientation in most models (1st and 3rd row), exceptions being the minimal inhibitory delay model and the model with most input noise. The standard model and blue noise input distribution model seem to have the strongest preference, while either increasing network size or adding noise reduces the preference somewhat. To compute phase distributions, only transition cells with positive gridness and an orientation between -5° and 5° were considered. Within a simulation, one of the qualifying transition cells was chosen as a reference, and the dots show the other qualifying transition cells' phase relative to their reference (rows 2 and 4). This phase was computed as the offset of the peak relative to the center in the cross correlogram between the transition cell and the reference.

One thought was that simulation times were too short for transition cells to develop the 7.5° orientation preference seen in previous simulations, but this did not seem to be the case (add some results indicating this?).

Phase distribution can only be investigated in simulation with minimally two cells sharing orientation, preferably more, and this was more common in larger networks. From looking at the networks with 23 or 37 transition cells, the phase distributions seem somewhat even, although the central area near the top of the rhomboid seems less populated (figure ref). Notedly, computing these phases was limited by the spatial resolution of the activity sampling, leading to rounding values.

It was briefly checked if the 37-cell networks had a toroidal structure in the population activity, which would be expected for grid cells belonging to the same module. This did not yield interesting results, and while it should be noted that those methods are created for larger networks, higher temporal resolution and rate-based network activity, it seems unlikely that networks with at most a third of the cells sharing orientation would have a highly ordered population activity structure.

3.4 Gridness spacing

All ten models introduced in section 3.1 used, barring noise, the same threshold for which spatial inputs would activate in a given location. Given a STDP-learning rule that lets an active transition cell decorrelate from less relevant spatial inputs, it would be expected that this relevance threshold is critical for the size of transition cell firing fields. That does not, however, mean that all models would give transition cells with the same spacing.

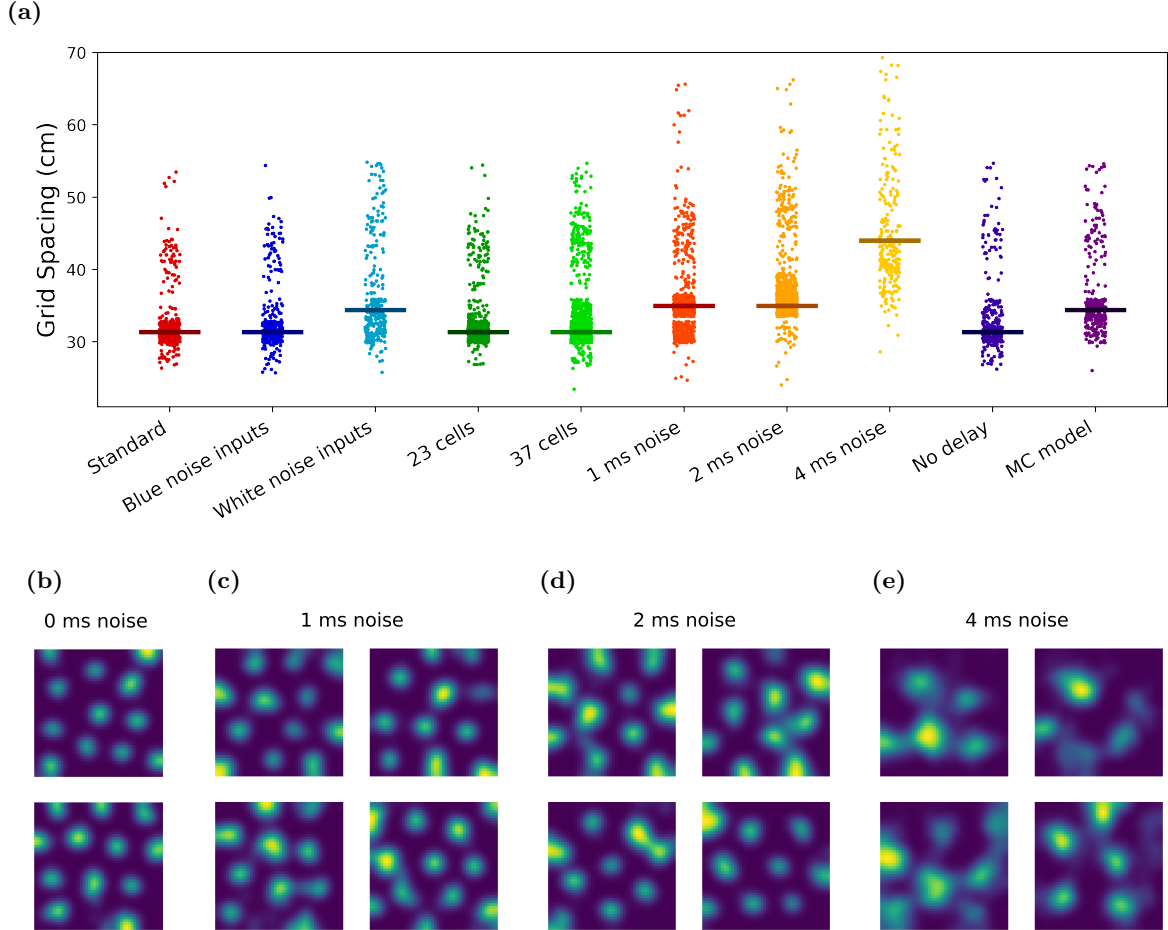


Figure 3.5: Grid spacing across ten models. This was computed as the spacing giving maximal gridness score for each cell after 95 simulation minutes. This was then filtered for cells with positive gridness. (a) Each dot represents the spacing in a single transition cell, sorted by model. Horizontal lines are model medians: for many models, the density is significantly higher close to the median than around. Notably, while mean spacing seems invariant on network size, adding noise seems to increase median spacing. Models with white noise inputs also had increased spacing, but that might be caused by poor gridness overall. Moreover, the multi-compartment model had higher spacing than the standard model. (b - e) Spike plots of models with identical parameters apart from input noise. (b) The standard model, without input noise, has a mean spacing of about 32.5 cm. As opposed to models with noise, transition cells can fit four firing fields horizontally in a 1×1 environment (lower spikeplot). (c & d) Models with 1 ms and 2 ms input noise have approximately similar mean spacing, at about 35 cm. (e) While 4 ms noise doesn't produce high gridness or clean firing fields, the average spacing is significantly larger than other models, with mean around 50 cm.

Curiously, while most models had highly similar spacing, which seems independent of input distribution and size of the transition cell layer (around 10.8 cm spacings), adding noise increased spacing, and it depended on amount of noise (figure 3.5). This was especially true for the highest noise level tested, with mean spacing at 50 cm, while the 1 ms and 2 ms models had an approximately 35 cm spacing preference.

3.5 Temporal stability

From earlier figures, it does seem like transition cells in many of the networks develop gridness over time, so the firing fields get more hexagonal over time. However, it is unclear if the fields converge on some stable configuration, or if they continuously shift throughout the simulation. Under the TSS model, transition cells with incremental, gradually improving hexagonality might be beneficial because transition cells also interconnect with place cells, so big changes in transition cell area will necessitate accurate changes in the connectivity between transition cells and place cells.

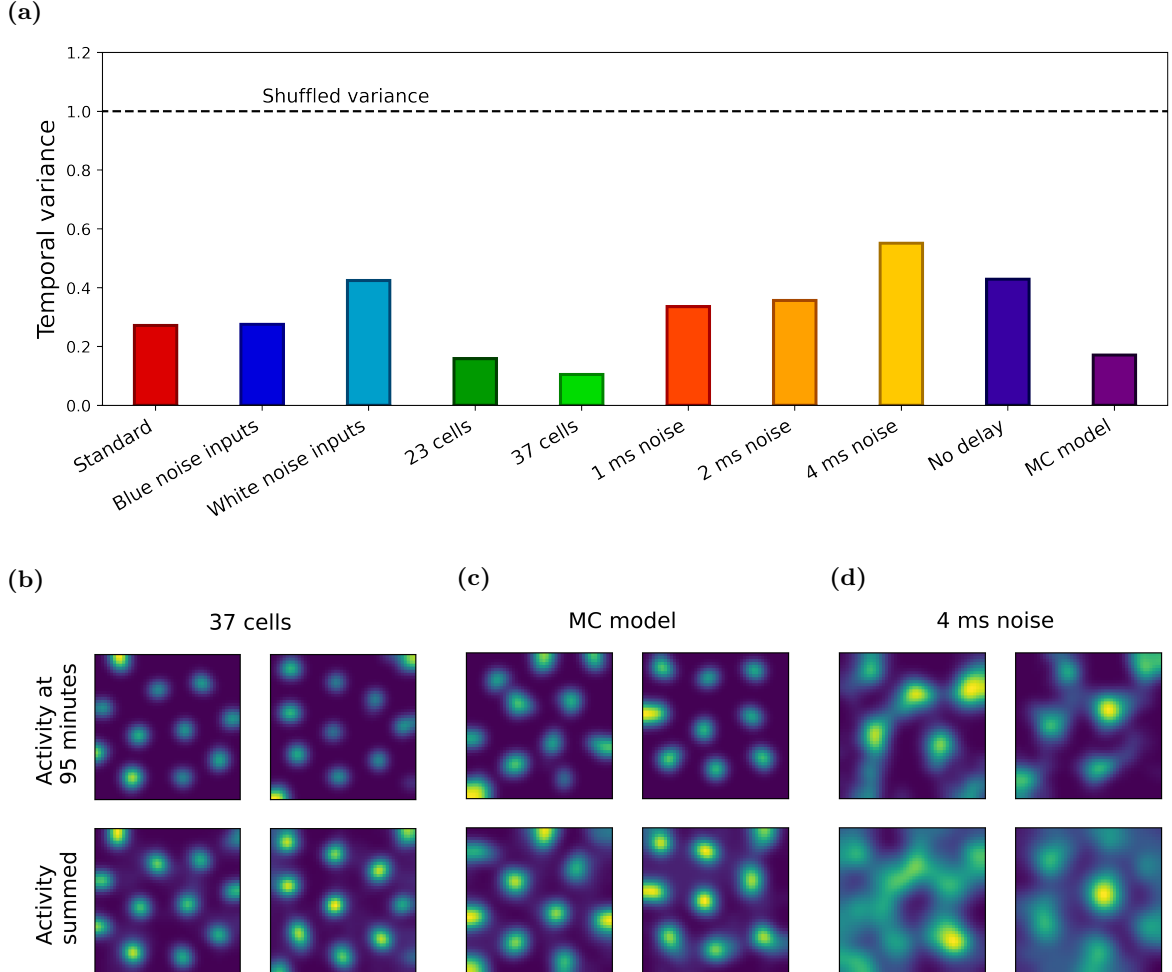


Figure 3.6: Temporal stability of different models. (a) The measure used to quantify temporal variance was the mean variance in spiking activity from one sampled time to the next, normalized by the variance in the shuffled data. A one in this score would indicate that there is no linear correlation between spiking from one sample time to the next, five simulation minutes later, while values close to zero indicate a positive correlation. Input noise seems to decrease temporal stability, while inhibitory delay seems to increase it. Larger networks also seem more resistant to change. (b - d) The 95 minute sample activity (row 1) and summed activity over all sample times (row 2) for three different models. All three models seem to have single-time samples with clear regions of activity and inactivity. The summed activity, however, shows that transition cells in the 37 transition cell model and the multi compartment model have maintained firing fields over time, while the noise model has not. This is reflected in their relative temporal variance scores.

To investigate this, a measure for temporal stability was used which tracks the transition cell activity in each of the sampled locations over time (figure 3.6 a). The measure is a temporal correlation, in which the variance from one sample to the next, taken five simulation minutes later, is compared to the variance with shuffled data. This shuffled variance is used as a standard for no

correlation, so a variance between 0 and 1 represents a positive temporal correlation, and variances above one is a negative correlation.

A positive correlation is clearly expected, because the input weights at one sampling time will be correlated to input weights at the next sampling. Additionally, the STDP learning rule is expected to encourage a cell to associate to some place and keep firing there. As such, the measure doesn't clearly indicate what should be understood as high temporal stability. Figures

3.6 (b - d) shows activity of two cells for three different models: the 37 transition cell model, which had the highest recorded stability, the 4 ms noise model with the lowest stability and the multi compartment model as an intermediate one. The first row in each plot shows the activity at the final sampled time, 95 minutes, while the second row shows the summarized activity over all times. The 4 ms noise model shows comparably homogenous summed activity relative to the single-time sample, which is expected of models with low temporal stability. The other two models, on the other hand, show clearly peaked summed activity. This is taken as an indication that these models, and models with comparable spatial stability, produce transition cells that maintain their firing fields over time, and can represent spatial transitions stably.

3.6 Multi-Compartment Models

One goal of this work was to investigate the nature of spatial inputs. While previous sections describes how transition cells can obtain hexagonal activity with place cell-like inputs, previous work assumed that this input was conveyed to the transition cell soma through active computation in a dendritic tree. The spatial inputs given to this dendritic tree could have some other form, such as boundary vectors. In this work, the dendritic tree was modelled as a multi-compartment method in which dendrites acted as perceptrons, receiving some input and activating according to a softmax function to activate the transition cell body.

The only model that has been presented so far in doing this was a highly simplified version, in which the spatial input was rectangularly distributed and place cell-like, and the dendritic layer was simply conveying this information directly to the soma in a non-spiking manner, as a proof of concept. This model performs somewhat similarly to the other models, but lacks a little in gridness (sections 3.2 - 3.5). An obstacle is that the addition of this intermediate dendrite layer increases simulation times significantly, so tuning parameters is slow.

Further efforts were made to move from this to a model taking boundary vector cell inputs. If dendrites should take BVC-inputs and convert them to place-like activity regions, this should be done in accordance to the previous results. Most importantly, if each dendrite responds to a single, random location independent of all other dendrites, the resulting dendritic tree might have a white-noise-like input distribution, which seems undesirable for these models.

With this in mind, the simplest BVC-model tried to replicate the rectangularly spaced inputs, so each dendrite received only two, orthogonal BVCs carefully tiled so each dendrite responds highly to a single position in a rectangular grid (figure 3.7 a, b). With this dual input, the dendrite stepwise activity would activate strongly when the input timing coincides, favoring places where both BVCs are equally far from their favored firing activity (figure 3.7 c). This gave dendrites a diagonal

cross-like firing field, which is different from the firing fields used in dendrites in the MC model.

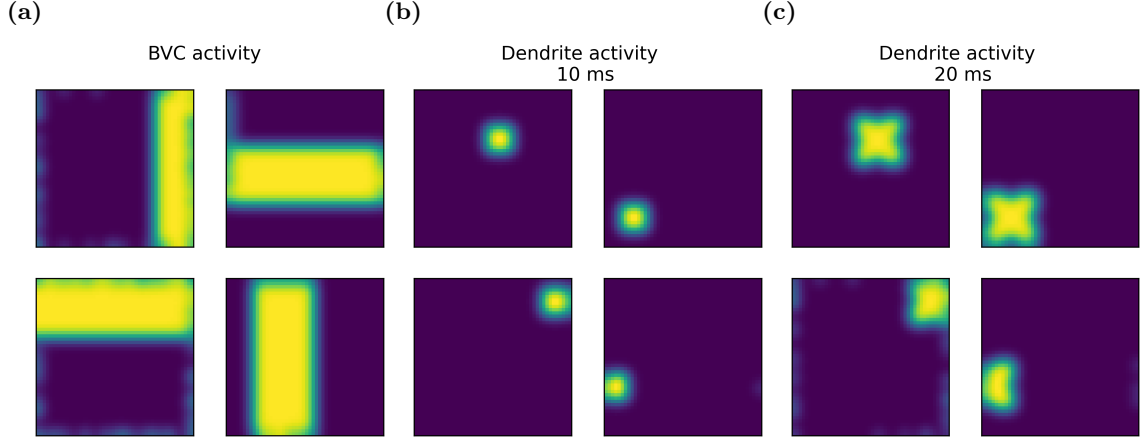


Figure 3.7: Boundary vector cell- and dendrite example activity during sampling. (a) In this model, all BVCs will align in one of the cardinal directions, giving them firing fields parallel to either the north/south walls or east/west walls. Distances were spaced linearly across the BVC population. (b) Dendrites would have an approximately circular firing fields at the intersection of their two input BVCs, if activity was limited to the first 10 ms after each theta cycle. (c) Across the entire time window, dendrites would activate in corners diagonal to their center of firing, places where their input would coincide at a significant delay. This limits the similarity between this model and the previous models.

Next to the place-preference of each dendrites in this model, an advantage is that the state of the network can be directly read out from the dendrite-to-transition cell weights, or their conductances, as it is known at simulation time which dendrite should be responsible for which place (figure 3.8 b). Although this model didn't develop overall positive gridness in test simulations, it did give transition cells with clear spatial firing fields (figure 3.8 a). Although this does not allow definitive conclusions on BVC as possible input structure, this shows some promise for this kind of model.

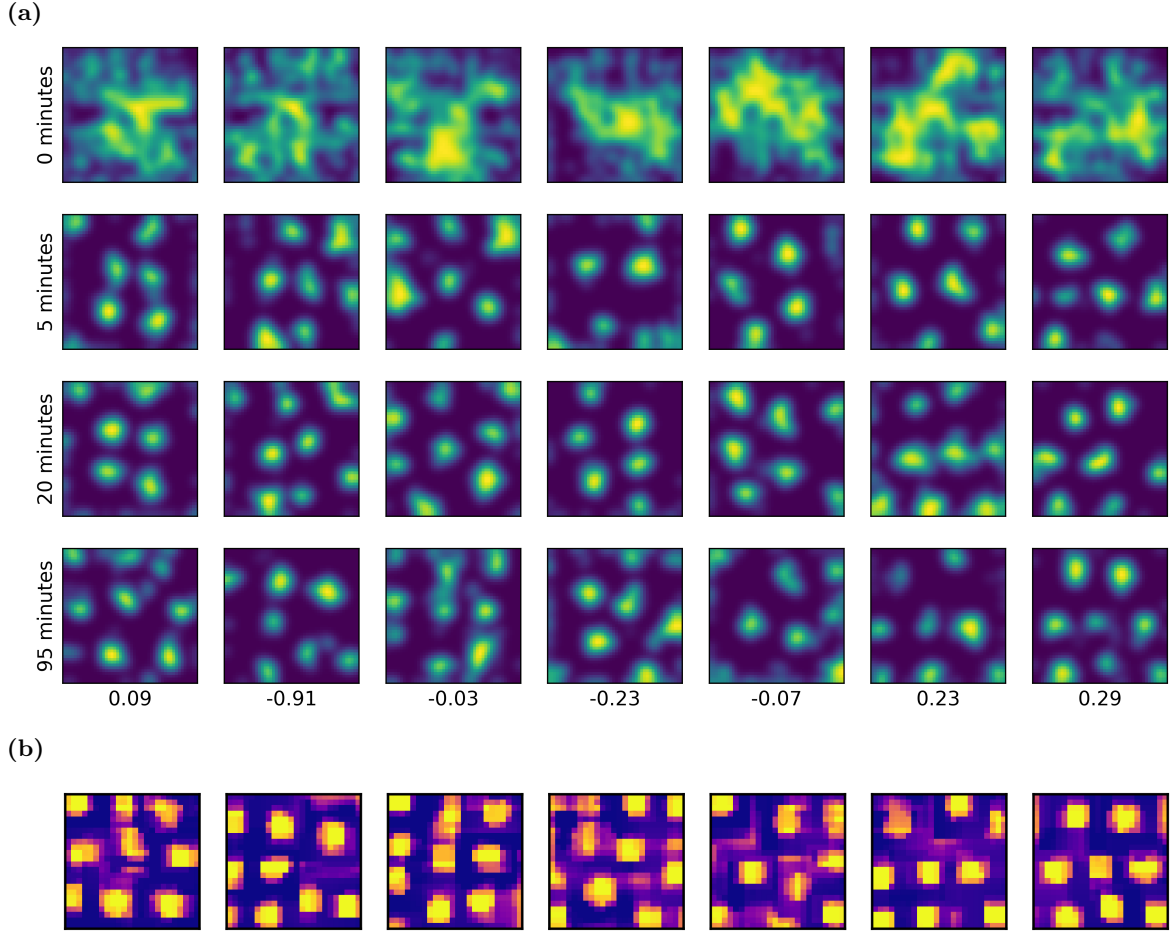


Figure 3.8: Preliminary results from BVC - models (a) Time series of sampled spike plots. Although the development of hexagonality isn't convincing, there are spatially separated firing fields. Each transition cell receives inputs from 24×24 dendrites, similar to the MC Model, but these dendrites receive input from a pair of orthogonal BVCs. (b) Dendrite-to-transition cell conductances from the bottom row in (a), sorted so each dendrite is placed in the intersection between the preferred firing fields of its two input BVCs.

4 Discussion

4.1 What this model shows

The goal of this work was to see how biologically plausible simulations of transition cells in the TSS model match experimental observations of entorhinal grid cells. Although studies on grid cells are numerous, some key variables were emphasized. First, that the network structure and morphology is reasonably close to the observed grid cell networks in the medial entorhinal cortex (mECII), so the transition cells are interconnected via strongly inhibiting interneurons. Secondly, that the activity pattern of the transition cells fit some criteria: most importantly that their firing was sufficiently hexagonal to pass as gridcells, and then that their firing properties follow that of single grid cell modules with similar grid spacings, a 7.5° wall-angle offset, and were reasonably temporally stable. On a population level, the criteria were arbitrarily large networks, uniformly distributed phases and a toroidal structure in the population activity. Finally, the spatial inputs given to grid cells should plausibly exist prior to learning a given environment, for instance driven by boundary vector cells, as opposed to place cells.

To match the TSS model, the transition cell layer would receive dense spatial inputs, and self-organize so each transition cell encodes as many spatial transitions as possible under a learning rule described in the TSS-model. This learning rule is based on two competing rules: first, that transition cells associate to central areas, where it encodes transitions from, to an annulus-shaped surrounding area where it encodes transitions to, and secondly that it tries to be active everywhere. This is a learning rule that leads, in theory, to optimally efficient transition cells.

The networks described in this model fits a majority of these requirements: the learning rule is in line with the TSS model, so the cells turn out as valid transition cells. This is coupled with networks that are reminiscent of the mECII grid cell network, which is characterized by strong lateral inhibition. It is not clear that that grid cells get spatially modulated input that is phase coded based on its relevance, but the theta-oscillations seen in the mEC shows some evidence of rhythmic activity. Importantly, the learning rule, given place-like inputs, produces transition cells with high levels of gridness, that share spacing across the population and show temporal stability. This is true for different network sizes, with 13, 23 or 37 transition cells, although gridness seems to fall for bigger networks. The network also holds up reasonably against noise, although it seems to depend on precision in the spatial inputs to a certain degree.

It is unclear if the network sees an upper limit in size, based on the fall in gridness in 37 cell networks. Getting high gridness has often been a case of setting parameters well, and if the parameter space giving high gridness shifts from changing network size, that would not have been caught in the simulations ran here. One example of this is that the reason all simulations here uses 24x24 inputs is because early simulations gave better results for these models than for 48x48 inputs, although the latter should strictly speaking simply increase model flexibility by increasing parameter count. This is discussed further in section 4.2.

Looking at single cell characteristics, there are two primary questions left open from the simulations run here: first, that very few simulations produced cells with unvaryingly high scores, instead often containing cells with low or even negative gridness. Secondly, that while transition cells seemed to coorganize with a single orientation, there seemed to be no preference for the empirically supported 7.5° wall angle offset. Instead, transition cells aligned perfectly with the wall.

Due to the universality of these problems - all models had large within-simulation variance in gridness score, and all models either preferred 0° wall angle offset or had little preferred orientation, and little improvement in longer simulations in both - there is reason to think that something is missing structurally, and not just that the parameters are wrong. Section 4.3 takes inspiration from other models on these topics, but examples on changes that could be made is varying inhibitory strength, as is seen in CAN models, or stronger transition cell dissociation with an interaction learning rule, as in the previous TSS-simulations.

While the models here supported networks of 37 transition cells, which developed reasonable gridness, cooriented with a 0° wall-angle offset and seemed to have uniform phase distribution, there was no evidence of population activity on a toroidal manifold. Existing literature shows how population activity within a grid cell module should represent the animal's position on a twisted torus (Gardner et al. 2022). However, the best simulation for this kind of work would be a single

37-cell simulation in which ten cells had positive gridness and an approximate 0° wall-angle offset, while the methods used to investigate this, inspired by (Gardner et al. 2022), depend on hundreds of grid cells. This would be an interesting line of study, but requires this model to be scaled up significantly. Additionally, new [unpublished?] observations suggest that the mEC grid cell network has a toroidal activity pattern even prior to any spatial exploration, which would put further restraint on this network structure.

Significant effort was made in this work to see how spatial inputs influence the transition cell network. An early goal was to use BVCs as inputs, and while this was never done convincingly here, some ideas at how this could be done was explored. These will be explored in the final subsection of this work, along with considerations on future work.

4.2 A word about parameters

As has been alluded to frequently throughout this work, simulating neural networks, and maybe particularly spiking neural networks, includes setting numerous parameters. Understanding what each parameter does is a tall order, considering their numerous interactions, which was for instance shown when networks with minimal inhibitory delay seemed to give good results, as opposed to previous simulations. Tuning learning parameters to make learning rules incrementing weights and learning rules decreasing weights somewhat balanced required time and experimentation. Increasing or decreasing network size, input size or spiking threshold changed simulation results thoroughly. Even if time hadn't been a constraint on this thesis, testing all parameter combinations would have been intractable.

With this in mind, it is worthwhile to stress that the majority of the results shown here are based on relatively little experimentation with parameters. White noise distributed inputs was more closely tested than the standard model and blue noise distributed input models, because of the perceived convenience completely unstructured inputs would represent. The fact that this model didn't produce high gridness, nonetheless, isn't a conclusive proof that it's impossible, but rather a sign that it's implausible - getting a transition cell network to achieve gridness is probably easier with more homogenous spatial input distributions.

4.3 Comparison to existing grid cell models

This work provides a network structure and learning rule that produces a cell-layer with grid-like activity from associating and dissociating to spatial inputs. Numerous other works has done this, each with their own set of assumptions. The benefit of feed-forward learning networks, compared to the popular CAN or OI -models, is that these models rely on external spatial information, and not self-velocity signals which can be prone to drift. That being said, there is rich support for CAN- and OI-models, and it is worth noting that these models are not directly antagonistic, instead seeking to explain different experimental grid cell observations. The major underlying assumption of this work, linking the observed grid cells to the theoretical transition cells of the TSS-model, is that grid cells receive spatial information in phase coded waves each theta cycle. From the perspective of TSS, phase coding the spatial relevance gives transition cell information about center- vs surround.

Biologically, the utility of phase coding the input activity is that it naturally orients with spike timing dependent plasticity as a biologically plausible learning rule. At least two criteria are necessary for biological plausibility; first, that all learning relies on spatially locally available information, and secondly, that learning only uses information that is available at the time of learning [source]. While STDP has been observed experimentally [source?], having baseline modulation of weights depends only on input-information. Compared to other models, the network does not rely on spike frequency adaptation [vs Kropff and Treves, for instance], and it does not rely on implausible learning rules such as backpropagation through time (BPTT) [source].

However, despite the reasonably good gridness observed in this network structure, the within-simulation variance is quite high, with virtually all simulations containing some cells with negative scores. This was also seen in another simulation combining inhibition and excitation [Weber and Sprekeler]. Although all cells showed clearly isolated firing fields, both asymmetry and rectangular firing fields will produce negative gridness. It does seem like the local minimum state for most cells is a hexagonal firing pattern, but that other configurations that give zero or negative scores are moderately likely with this learning rule, possibly even necessary in a network. Additionally, from the temporal stability of the firing fields, there is indication that the cells with negative scores will be known early in the simulation, and only persist in their negative scores (can data support this?).

4.4 Comparison with existing TSS simulations

Transition cells, under the TSS-model, learn spatial transitions by associating to spatial information related to center-regions they encode transitions from, and dissociating from spatial information related to surround-regions, which they encode transitions to. A mechanism to support this is dense sampling, in which, in any given position, both spatial information from the places corresponding to center and the surround will be available [source: TSS thesis?]. This lets the transition cell acquaint to all spatial information, which is necessary to subsequently represent spatial transitions. Transition neurons also communicate laterally with inhibition, to discourage overlapping fields and representing the same transitions. Prior to this work, all simulations of spatial learning under the TSS-model had unresolved questions that needed to be answered to be applicable in a biological network: how could a high number of transition neurons coexist in the network, and what would a biologically plausible learning rule look like? In the original simulations, inhibition times were instant, rate of learning was modulated by the number of inputs to account for edge effects, and the only input structure tested was one with a rectangular distribution. Compared to this, this work is a decisive step in the direction of biological plausibility, showing high degrees of gridness in larger networks, as well as uniform phase distributions. Although this work did not show explicit hexagonality with BVC-inputs, it showed gridness with different input distributions, a smaller number of dendrites (576 vs 2304) and only velocity-based learning rate modulation.

Existing simulations of the TSS model had a third learning rule, an interaction rule, in which transition cells dissociated from spatial information whenever another transition cell activated first. This learning rule wasn't implemented here because it wasn't clear how - one plausible alternative is that receiving inhibition would decrease weights, but this was technically difficult to implement with

the simulation library used, and would have increased simulation times. However, a learning rule like this might encourage faster convergence and a wall-angle orientation closer to the 7.5 degrees that might be expected, due to its high number of packed center-surround areas. On the other hand, this learning rule might also strain the network more in terms of size, because it discourages overlapping fields.

4.5 The future: benefits of BVCs, biological plausibilities etc

Considering that optic flow can explain boundary vector cell activity from pure visual inputs, a network producing gridlike cells from BVC-inputs is desirable because it explains how spatial transitions can be learnt from sensory information available at the time of exploration. Under certain conditions, it might also extrapolate to other vector-based inputs, such as object-vector cells, given that these cells can also be modeled from optic flow, and that there is a sufficient number of landmarks to triangulate positional information from. Although this work by no means is conclusive on the nature of such a network, nor any concrete data on the BVC-to-transition cell network, it provides some predictions at what such a network should look like.

Importantly, because most BVCs will be active in both the center- and the surround-region of the transition cell [supplementary models, I guess], linear summation of all boundary vector cell activity is unlikely to yield effective transition cells. Instead, some nonlinear process is necessary to allow transition cells to respond to BVCs in some locations, and not in others. In this work, the mechanism that supports this is dendritic computations, in which each dendrite receives a subset of BVC-inputs, and the transition cell in practice can learn on each dendrite, instead of individual inputs. This idea followed both experimental data on superlinear activation of pyramidal grid cell dendrites [source], as well as a model using dendritic computations to explain place cell remapping [source]. In this model, each dendrite adapted to some place in some environment, and context-signals would inhibit all dendrites except the one governing the current environment. This allowed the place cell to remap orthogonally.

Using the same idea in this work, so each dendrite would represent some location in the environment, the learning variable was the dendrite conductance, and not synaptic weights. This isn't grounded in experimental observations, but rather two reasons of model clarity: first, that this mimics models in which place-like spatial inputs synapse onto grid cells, such as the other models in this work. This clarifies comparison, because the learning variable always has the same functional role in the network, as place-input to grid-cell weights. Secondly, although not directly explored here, one way of self-organizing BVC- to dendrite-connectivity is by randomly connecting a superfluous number of BVCs on each dendrite, and pruning unnecessary connections so the dendrite activates in only one or a few places. Differentiating between these two kinds of learning - BVC-to-dendrite and dendrite-to-grid cell, was thought to make these processes easier to distinguish. This model provides the testable hypothesis that 1) dendrites will exhibit place-like activity fields during traversing of familiar environments, and 2) only depolarization in dendrites which represent places that are within the hexagonal grid pattern will contribute to somatic depolarization and grid cell spiking.

That being said, there is no central limitation that learning has to occur in dendrite-to-grid cell

conductances. Alternatively, the STDP-learning signal must be transmitted to all postsynapses in the dendrite, in which all the weights will be changed indiscriminately, except possibly those pruned in mechanisms described in the above paragraph. In this case, it is also possible that all dendrites end up with place fields within the grid pattern.

One of the most direct predictions from this work is that in the case of such a dendritic input tree, the distribution of place-like inputs to the grid cell should be relatively evenly distributed spatially. With LIF model neurons, it seems more difficult to converge on proper gridness when inputs have place fields that are uniformly and independently distributed. A more even distribution, such as a blue noise pattern, is for instance seen in the layout of cones in the human retina, but to make dendrites activate in a blue noise pattern would require some mechanism, for instance by making them disassociate from each other.

Some further challenges underlie the model relying on an expansive dendritic tree as a hidden layer between vectorized inputs and grid-like transition cells. Not only is the number of dendrites required too high compared to that of both stellate and pyramidal principal mECII cells, but if each dendrite should correspond to one location, the required number of dendrites required would need to scale linearly with the number of places visited. If inspiration is again taken from what is known of hippocampal place cells, some kind of context modulation or remapping might help explain this, but significant work is required to highlight how this would work. With BVC-input, the same dendrite would in principle respond to the same place in multiple environments, as long as the boundary information is similar, so each dendrite could be reused across contexts as long as conductances could be modulated across environments. Prior to exploring this in the engineer-like simulations like this work has done, this question should be investigated in a theoretical framework. It is, however, in the spirit of the TSS to assume that the dendrites of a transition cell serves some computational purpose, and does this well.

References

- Tolman, Edward C., B. F. Ritchie, and D. Kalish (1946). "Studies in Spatial Learning. I. Orientation and the Short-cut". In: *Journal of Experimental Psychology* (36), p. 13. DOI: <https://doi.org/10.1037/h0053944>.
- Tolman, Edward C. (1948). "Cognitive Maps in Rats and Men". In: *Psychological Review* (55), pp. 189 –208.
- O'Keefe, John (1976). "Place units in the hippocampus of the freely moving rat". In: *Experimental Neurology* 51.1, pp. 78–109. ISSN: 0014-4886. DOI: [https://doi.org/10.1016/0014-4886\(76\)90055-8](https://doi.org/10.1016/0014-4886(76)90055-8). URL: <https://www.sciencedirect.com/science/article/pii/0014488676900558>.
- O'Keefe, John and Jonathan O. Dostrovsky (1976). "The hippocampus as a spatial map: Preliminary evidence from unit activity in the freely-moving rat." In: *Brain Research*, pp. 171–175. DOI: [https://doi.org/10.1016/0006-8993\(71\)90358-1](https://doi.org/10.1016/0006-8993(71)90358-1).

- Etienne, Ariane S. (Sept. 1980). "The orientation of the golden hamster to its nest-site after the elimination of various sensory cues". In: *Cellular and Molecular Life Sciences* 36, pp. 1048–1050. DOI: <https://doi.org/10.1007/BF01965961>.
- Suzuki, Shinya, Gerda Augerinos, and Abraham H. Black (Feb. 1980). "Stimulus control of spatial behavior on the eight-arm maze in rats". In: *Learning and Motivation* 11, pp. 1–18. DOI: [https://doi.org/10.1016/0023-9690\(80\)90018-1](https://doi.org/10.1016/0023-9690(80)90018-1).
- Muller, Robert U. and John L. Kubie (July 1987). "The Effects of Changes in the Environment on the Spatial Firing of Hippocampal Complex-Spike Cells". In: *The Journal of Neuroscience* 7, pp. 1951–1968. DOI: <https://doi.org/10.1523/JNEUROSCI.07-07-01951.1987>.
- Groenand, Thomas van and J. Michael Wyss (June 1990). "The connections of presubiculum and parasubiculum in the rat". In: *Brain Research* 518, pp. 227 –243. DOI: [https://doi.org/10.1016/0006-8993\(90\)90976-I](https://doi.org/10.1016/0006-8993(90)90976-I).
- O'Keefe, John and Michael L. Reese (July 1993). "Phase relationship between hippocampal place units and the EEG theta rhythm". In: *Hippocampus* 3 (3), pp. 317 –330. DOI: <https://doi.org/10.1002/hipo.450030307>.
- Tamamaki, Nobuaki and Yoshiaki Nojyo (Oct. 1993). "Projection of the entorhinal layer II neurons in the rat as revealed by intracellular pressure-injection of neurobiotin". In: *Hippocampus* 3, pp. 471 –480. DOI: <https://doi.org/10.1002/hipo.450030408>.
- Wilson, Matthew A. and Bruce L. McNaughton (1993). "Dynamics of the Hippocampal Ensemble Code for Space". In: *Science* 261.5124, pp. 1055–1058. DOI: 10.1126/science.8351520. eprint: <https://www.science.org/doi/pdf/10.1126/science.8351520>. URL: <https://www.science.org/doi/abs/10.1126/science.8351520>.
- (1994). "Reactivation of Hippocampal Ensemble Memories During Sleep". In: *Science* 265.5172, pp. 676–679. DOI: 10.1126/science.8036517. eprint: <https://www.science.org/doi/pdf/10.1126/science.8036517>. URL: <https://www.science.org/doi/abs/10.1126/science.8036517>.
- Skaggs, William E. et al. (1996). "Theta phase precession in hippocampal neuronal populations and the compression of temporal sequences". In: *Hippocampus* 6 (2), pp. 149–172. DOI: [https://doi.org/10.1002/\(SICI\)1098-1063\(1996\)6:2<149::AID-HIPO6>3.0.CO;2-K](https://doi.org/10.1002/(SICI)1098-1063(1996)6:2<149::AID-HIPO6>3.0.CO;2-K).
- Hafting, Torkild et al. (Aug. 2005). "Microstructure of a spatial map in the entorhinal cortex". In: *Nature*, pp. 801–806. DOI: <https://doi.org/10.1038/nature03721>.
- Kunsch, H.R., E. Agrell, and F.A. Hamprecht (2005). "Optimal lattices for sampling". In: *IEEE Transactions on Information Theory* 51.2, pp. 634–647. DOI: 10.1109/TIT.2004.840864.
- Barry, Caswell et al. (Jan. 2006). "The Boundary Vector Cell Model of Place Cell Firing and Spatial Memory". In: *Reviews in the Neurosciences* 17.1-2. ISSN: 0334-1763. DOI: 10.1515/revneuro.2006.17.1-2.71. URL: <http://dx.doi.org/10.1515/revneuro.2006.17.1-2.71>.
- Burgess, Neil, Caswell Barry, and John O'Keefe (2007). "An oscillatory interference model of grid cell firing". In: *Hippocampus* 17.9, pp. 801–812. DOI: <https://doi.org/10.1002/hipo.20327>. eprint: <https://onlinelibrary.wiley.com/doi/pdf/10.1002/hipo.20327>. URL: <https://onlinelibrary.wiley.com/doi/abs/10.1002/hipo.20327>.

- Furtak, Sharon C. et al. (Aug. 2007). "Functional Neur'anatomy of the Parahippocampal Region in the Rat: The Perirhinal and Postrhinal Cortices". In: *Hippocampus* 17, pp. 709 –722. DOI: <https://doi.org/10.1002/hipo.20314>.
- Kerr, Kristin M. et al. (Aug. 2007). "Functional Neuroanatomy of the Parahippocampal Region: The Lateral and Medial Entorhinal Areas". In: *Hippocampus* 17, pp. 697 –708. DOI: <https://doi.org/10.1002/hipo.20315>.
- Hafting, Torkel et al. (2008). "Hippocampus-independent phase precession in entorhinal grid cells". In: *Nature* 453, pp. 1248–1252. DOI: <https://doi.org/10.1038/nature06957>.
- Kropff, Emilio and Alessandro Treves (2008). "The emergence of grid cells: Intelligent design or just adaptation?" In: *Hippocampus* 18.12, pp. 1256–1269. DOI: <https://doi.org/10.1002/hipo.20520>. eprint: <https://onlinelibrary.wiley.com/doi/pdf/10.1002/hipo.20520>. URL: <https://onlinelibrary.wiley.com/doi/abs/10.1002/hipo.20520>.
- Boccara, Charlotte N et al. (July 2010). "Grid cells in pre- and parasubiculum". In: *Nature* 13, pp. 987–994. DOI: <https://doi.org/10.1038/nrn.2602>.
- Dudchenko, Paul A. (2010). *Why People Get Lost: The Psychology and Neuroscience of Spatial Cognition*. Oxford: Oxford University Press. DOI: <https://doi.org/10.1093/acprof:oso/9780199210862.001.0001>.
- Langston, Rosamund F. et al. (2010). "Development of the Spatial Representation System in the Rat". In: *Science* 328.5985, pp. 1576–1580. DOI: [10.1126/science.1188210](https://doi.org/10.1126/science.1188210). eprint: <https://www.science.org/doi/pdf/10.1126/science.1188210>. URL: <https://www.science.org/doi/abs/10.1126/science.1188210>.
- Wills, Tom J. et al. (2010). "Development of the Hippocampal Cognitive Map in Preweanling Rats". In: *Science* 328.5985, pp. 1573–1576. DOI: [10.1126/science.1188224](https://doi.org/10.1126/science.1188224). eprint: <https://www.science.org/doi/pdf/10.1126/science.1188224>. URL: <https://www.science.org/doi/abs/10.1126/science.1188224>.
- Zilli, Eric A. and Michael E. Hasselmo (2010). "Coupled Noisy Spiking Neurons as Velocity-Controlled Oscillators in a Model of Grid Cell Spatial Firing". In: *Journal of Neuroscience* 30.41, pp. 13850–13860. ISSN: 0270-6474. DOI: [10.1523/JNEUROSCI.0547-10.2010](https://doi.org/10.1523/JNEUROSCI.0547-10.2010). eprint: <https://jneurosci.org/content/30/41/13850.full.pdf>. URL: <https://www.jneurosci.org/content/30/41/13850>.
- Brandon, Mark P. et al. (2011). "Reduction of Theta Rhythm Dissociates Grid Cell Spatial Periodicity from Directional Tuning". In: *Science* 332.6029, pp. 595–599. DOI: [10.1126/science.1201652](https://doi.org/10.1126/science.1201652). eprint: <https://www.science.org/doi/pdf/10.1126/science.1201652>. URL: <https://www.science.org/doi/abs/10.1126/science.1201652>.
- Dragoi, George and Susumu Tonegawa (Jan. 2011). "Preplay of future place cell sequences by hippocampal cellular assemblies". In: *Nature* 469, pp. 397–401. DOI: <https://doi.org/10.1038/nature09633>.
- Koenig, Julie et al. (2011). "The Spatial Periodicity of Grid Cells Is Not Sustained During Reduced Theta Oscillations". In: *Science* 332.6029, pp. 592–595. DOI: [10.1126/science.1201685](https://doi.org/10.1126/science.1201685). eprint:

- <https://www.science.org/doi/pdf/10.1126/science.1201685>. URL: <https://www.science.org/doi/abs/10.1126/science.1201685>.
- Yartsev, Michael M., Menno P. Witter, and Nachum Ulanovsky (Nov. 2011). “Grid cells without theta oscillations in the entorhinal cortex of bats”. In: *Nature* 479, pp. 103–107. DOI: <https://doi.org/10.1038/nature10583>.
- Raudies, Florian and Michael E. Hasselmo (June 2012). “Modeling Boundary Vector Cell Firing Given Optic Flow as a Cue”. In: *PLOS Computational Biology* 8.6, pp. 1–17. DOI: [10.1371/journal.pcbi.1002553](https://doi.org/10.1371/journal.pcbi.1002553). URL: <https://doi.org/10.1371/journal.pcbi.1002553>.
- Stensola, Hanne et al. (Dec. 2012). “The entorhinal grid map is discretized”. In: *Nature*, pp. 72 –78. DOI: <https://doi.org/10.1038/nature11649>.
- Wills, Tom J., Caswell Barry, and Francesca Cacucci (2012). “The abrupt development of adult-like grid cell firing in the medial entorhinal cortex”. In: *Frontiers in Neural Circuits* 6. ISSN: 1662-5110. DOI: [10.3389/fncir.2012.00021](https://doi.org/10.3389/fncir.2012.00021). URL: <https://www.frontiersin.org/articles/10.3389/fncir.2012.00021>.
- Zilli, Eric (2012). “Models of Grid Cell Spatial Firing Published 2005–2011”. In: *Frontiers in Neural Circuits* 6. ISSN: 1662-5110. DOI: [10.3389/fncir.2012.00016](https://doi.org/10.3389/fncir.2012.00016). URL: <https://www.frontiersin.org/articles/10.3389/fncir.2012.00016>.
- Bonnevie, Tora et al. (Mar. 2013). “Grid cells require excitatory drive from the hippocampus”. In: *Nature Neuroscience*, pp. 309–317. DOI: <https://doi.org/10.1038/nn.3311>.
- Couey, Jonathan J et al. (Mar. 2013). “Recurrent inhibitory circuitry as a mechanism for grid formation”. In: *Nature Neuroscience*, pp. 318–324. DOI: <https://doi.org/10.1038/nn.3310>.
- Dragoi, George and Susumu Tonegawa (May 2013). “Distinct preplay of multiple novel spatial experiences in the rat”. In: *PNAS*. DOI: <https://doi.org/10.1073/pnas.1306031110>.
- Si, Bailu and Alessandro Treves (Aug. 2013). “A model for the differentiation between grid and conjunctive units in medial entorhinal cortex”. In: *Hippocampus* 23, pp. 1410 –1424. DOI: <https://doi.org/10.1002/hipo.22194>.
- Yoon, KiJung et al. (July 2013). “Specific evidence of low-dimensional continuous attractor dynamics in grid cells”. In: *Nature Neuroscience* 16, pp. 1077–1084. DOI: <https://doi.org/10.1038/nn.3450>.
- Buetfering, Christina, Kevin Allen, and Hannah Monyer (May 2014). “Parvalbumin interneurons provide grid cell-driven recurrent inhibition in the medial entorhinal cortex”. In: *Nature Neuroscience*, pp. 710–718. DOI: <https://doi.org/10.1038/nn.3696>.
- Castro, Luisa and Paulo Aguiar (Apr. 2014). “A feedforward model for the formation of a grid field where spatial information is provided solely from place cells”. In: *Biological Cybernetics* 108, pp. 133–143. DOI: <https://doi.org/10.1007/s00422-013-0581-3>.
- Widloski, John and Ila R. Fiete (2014). “A Model of Grid Cell Development through Spatial Exploration and Spike Time-Dependent Plasticity”. In: *Neuron* 83.2, pp. 481–495. ISSN: 0896-6273. DOI: <https://doi.org/10.1016/j.neuron.2014.06.018>.
- Cherubini, Enrico and Richard Miles (2015). “The CA3 region of the hippocampus: how is it? what is it for? how does it do it?” In: *Frontiers in Cellular Neuroscience* 9. ISSN: 1662-5102. DOI:

- 10.3389/fncel.2015.00019. URL: <https://www.frontiersin.org/articles/10.3389/fncel.2015.00019>.
- Krupic, Julija et al. (Feb. 2015). “Grid cell symmetry is shaped by environmental geometry”. In: *Nature*, pp. 232–235. DOI: <https://doi.org/10.1038/nature14153>.
- Stensola, Tor et al. (Feb. 2015). “Shearing-induced asymmetry in entorhinal grid cells”. In: *Nature*, pp. 207–212. DOI: <https://doi.org/10.1038/nature14151>.
- Mulas, Marcello, Nicolai Waniek, and Jorg Conradt (2016). “Hebbian Plasticity Realigns Grid Cell Activity with External Sensory Cues in Continuous Attractor Models”. In: *Frontiers in Computational Neuroscience* 10. DOI: <https://doi.org/10.3389/fncom.2016.00013>.
- Olafsdottir, H Freyja, Francis Carpenter, and Caswell Barry (June 2016). “Coordinated grid and place cell replay during rest”. In: *Nature Neuroscience*, pp. 792–794. DOI: <https://doi.org/10.1038/nn.4291>.
- Waniek, Nicolai (2017). “Multi-Transition Systems: A theory for neural spatial navigation”. In: *BioRxiv*. DOI: <https://doi.org/10.1101/174946>.
- Witter, Menno P. et al. (2017). “Architecture of the Entorhinal Cortex A Review of Entorhinal Anatomy in Rodents with Some Comparative Notes”. In: *Frontiers in Systems Neuroscience* 11. DOI: <https://doi.org/10.3389/fnsys.2017.00046>.
- Rowland, David C et al. (Sept. 2018). “Functional properties of stellate cells in medial entorhinal cortex layer II”. In: *eLife*. DOI: <https://doi.org/10.7554/eLife.36664>.
- Waniek, Nicolai (2018). “Hexagonal Grid Fields Optimally Encode Transitions in Spatiotemporal Sequences”. In: *Neural Computation* (30), pp. 2691–2725. DOI: https://doi.org/10.1162/neco_a_01122.
- Stimberg, Marcel, Romain Brette, and Dan F. M. Goodman (2019). “Brian2, an intuitive and efficient neural simulator”. In: *eLife* 8. DOI: <https://doi.org/10.7554/eLife.47314>.
- Monsalve-Mercado, Mauro M. and Christian Leibold (Oct. 2020). “Effect of boundaries on grid cell patterns”. In: *Physiological Review Research* 2. DOI: <https://doi.org/10.1103/PhysRevResearch.2.043137>.
- Waniek, Nicolai (2020). “Transition Scale-Spaces; A Computational Theory for the Discretized Entorhinal Cortex”. In: *Neural Computation* (32), pp. 330–394. DOI: https://doi.org/10.1162/neco_a_01255.
- Christensen, Ane Charlotte et al. (Jan. 2021). “Perineuronal nets stabilize the grid cell network”. In: *Nature Communications*, p. 253. DOI: <https://doi.org/10.1038/s41467-020-20241-w>.
- Soldatkina, Oleksandra, Francesca Schonsberg, and Alessandro Treves (Oct. 2021). “Challenges for Place and Grid Cell Models”. In: *Computational Modelling of the Brain* 1359, pp. 285 –312. DOI: <https://doi.org/10.1007/97>.
- Gardner, Richard J. et al. (Feb. 2022). “Toroidal topology of population activity in grid cells”. In: *Nature*, pp. 123–128. DOI: <https://doi.org/10.1038/s41586-021-04268-7>.
- George, Tom M. et al. (2024). “RatInABox, a toolkit for modelling locomotion and neuronal activity in continuous environments”. In: *eLife* 13. DOI: <https://doi.org/10.7554/eLife.85274>.